# The Ozonolysis of α-Terpineol in an Aqueous Environment: A Model for Atmospheric Cloud Chemistry

Dani Leviss

May 2016

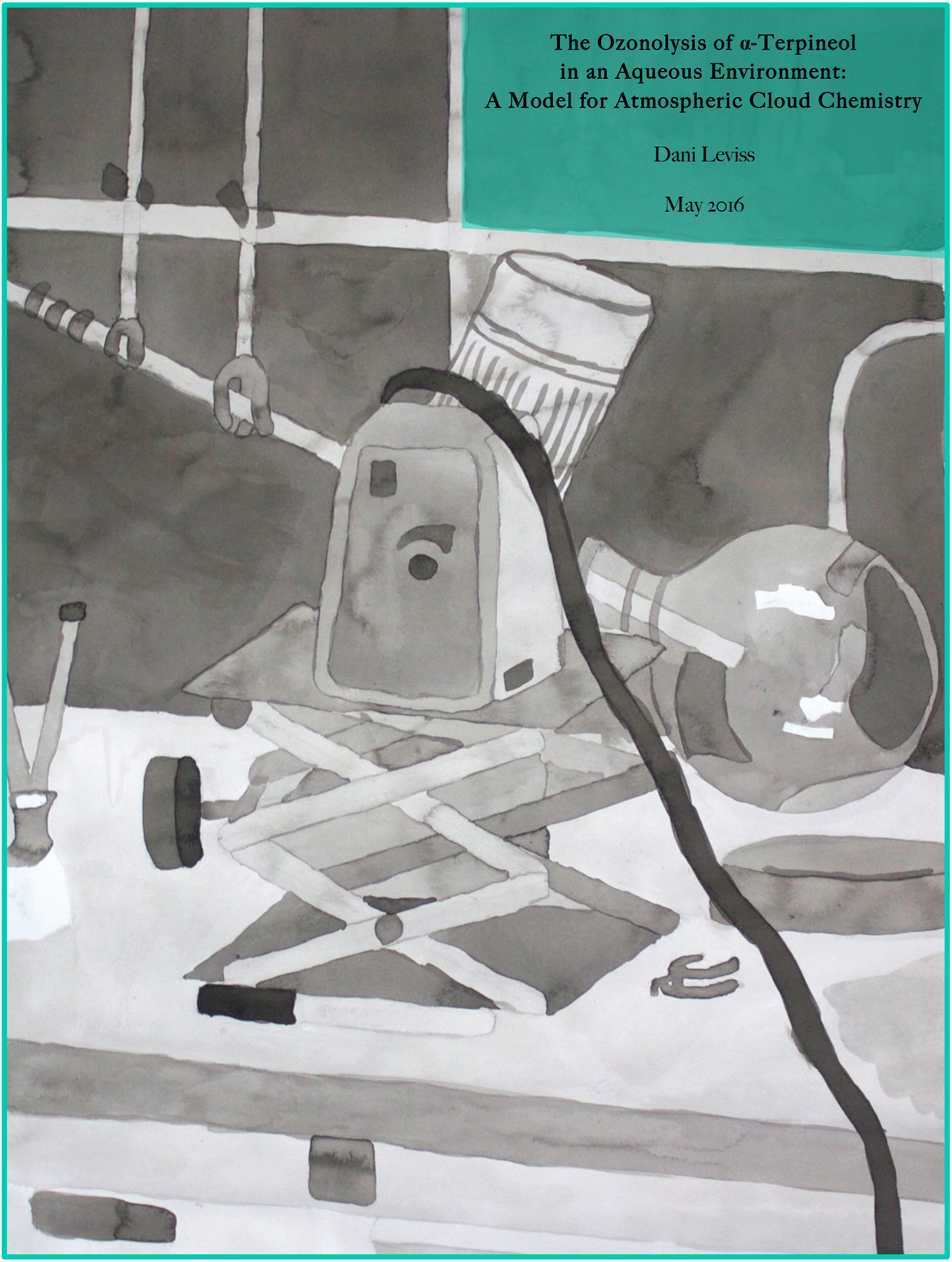

Drew University
College of Liberal Arts

# The Ozonolysis of α-Terpineol in an Aqueous Environment: A Model for Atmospheric Cloud Chemistry

A Thesis in Chemistry
by
Dani Leviss

Submitted in Partial Fulfillment
of the Requirements
for the Degree of
Bachelor in Arts
With Specialized Honors in Chemistry

May 2016

**A Note on the Cover Illustration**

The water and ink illustration on the cover is the middle panel of a triptych I created at Drew in Spring 2015 in the course Drawing II. The triptych depicts three aspects of my experience at Drew—art, science, and writing. The left panel is a drawing of the entrance to the Arts wing of the Dorothy Young Center for the Arts, with charcoal as the medium since it is a commonly used drawing material. The middle panel features the experimental setup I used to conduct my research. Water and ink symbolize the aqueous phase of the reaction I've studied. The right panel combines charcoal and ink in an illustration of The Acorn office, which has been my Thursday night home for the last four years and where I've developed my writing and journalism skills. Both charcoal and ink were used to reflect the combining of my areas of study and also my future goals of creatively communicating about science in the writing and journalism fields.

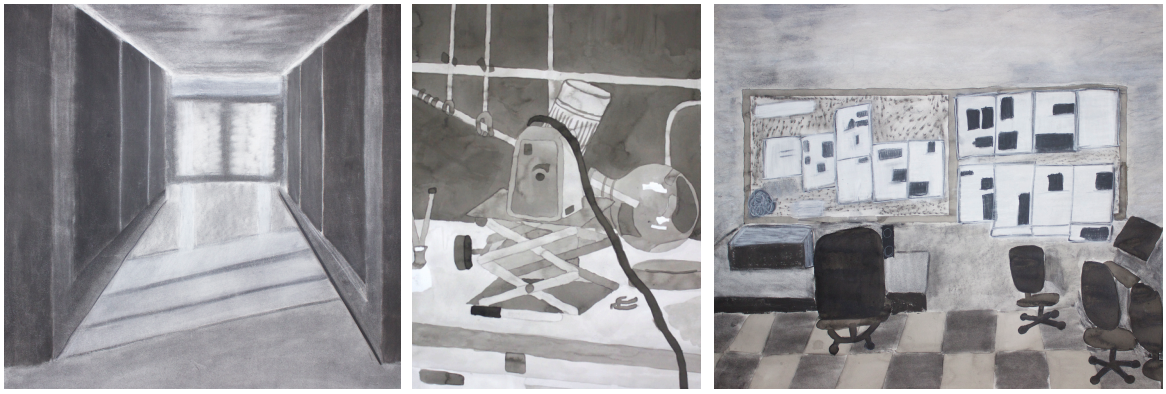

Leviss, D., *Untitled*, 2015. Charcoal and ink, 64 in x 22 in. Drew University.

**Acknowledgements**

I am sincerely thankful for the mentorship and support of my research advisor, Dr. Ryan Hinrichs who encouraged me to stay hopeful with the project when the path was unclear and without whom this project would never exist. I am grateful for the helpful guidance of my committee members. Dr. Alan Rosan, thank you for your invaluable organic chemistry insight. Dr. Summer Harrison, thank you for introducing me to the intersection of climate change and human rights and encouraging optimism about Earth's future. Dr. Hilary Kalagher, thank you for serving as the chair of my committee and for your outside perspective during the writing process.

I would also like to thank Daryl Van Ry for his Gas Chromatography-Mass Spectrometry expertise and help in unlocking the identifications of the products. Dr. Andy Evans, thank you for your Nuclear Magnetic Resonance Spectroscopy expertise, especially with two-dimensional NMR and theoretical NMR. I thank Margery Ashmun, Drew's science reference librarian, for providing her research detective skills. I would like to thank Dr. Mary-Ann Pearsall for advising me during my four years at Drew and encouraging me to write an honors thesis.

Thank you to my friends and family for listening to me talk about my research and supporting me through every frustration and triumph. I am especially grateful for the encouragement and friendship of Miho Watabe throughout the last three years. Finally, I would like to thank Drew University, its chemistry department, and the Drew Summer Science Institute for providing the opportunity to conduct research and the National Science Foundation for providing financial support.

**Abstract**

Ozone is a major atmospheric pollutant, a central component of smog, a lung irritant, and able to react with abundant organic atmospheric aerosols. The gas phase ozonolysis of volatile organic compounds has been extensively studied and shown to be a major pathway for the formation of secondary organic aerosol (SOA). Although recent work indicates that aqueous processes account for a major fraction of SOA, little is known about aqueous phase ozonolysis. In the present research, we studied the ozonolysis of α-terpineol in aqueous solutions to model the chemistry of atmospheric droplets at varied ozone concentrations (131, 480, and 965 ppb). $^{1}$H Nuclear Magnetic Resonance Spectroscopy (NMR) monitored the experimental progress of this reaction, and one- and two-dimensional NMR along with Gas Chromatography-Mass Spectrometry (GCMS) and Infrared Spectroscopy (IR) identified products.

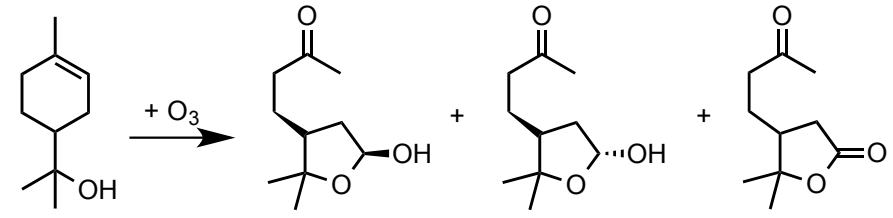


The second-order rate coefficient of the aqueous reaction is 9.93 x $10^{6}$ $M^{-1}s^{-1}$ with a lifetime of 5.2 min, 15 times shorter than in the gas phase (lifetime of 79 min). Formation of products of decreased volatility suggests ozonolysis of α -terpineol yields more condensible secondary organic material and therefore potentially increased impact on climate, visibility, and health.

## Table of Contents

## List of Figures, Schemes, and Tables

### Figures

**Schemes**

**Tables**

## List of Abbreviations

| | |
|---|---|
| ATR-FTIR | Attenuated Total Reflectance-Fourier Transform Infrared Spectroscopy |
| CCN | Cloud Condensation Nuclei |
| CI | Criegee Intermediate |
| COSY | Correlation Spectroscopy, a 2-D NMR experiment |
| DRIFTS | Diffuse Reflectance Infrared Spectroscopy |
| FID | Free Induction Decay |
| FMO | Frontier Molecular Orbital |
| GCMS | Gas Chromatography/Mass Spectrometry |
| GIAO | Gauge-Independent Atomic Orbital |
| HOMO | Highest Occupied Molecular Orbital |
| HSQC | Heteronuclear Single Quantum Correlation Spectroscopy, a 2-D NMR experiment |
| IR | Infrared Spectroscopy |
| LUMO | Lowest Unoccupied Molecular Orbital |
| NIST | National Institute of Standards and Technology |
| NMR | Nuclear Magnetic Resonance Spectroscopy |
| PCM | Polarizable Continuum Model |
| PM | Particulate Matter |
| POZ | Primary Ozonide |
| RF | Radiative Forcing |
| RT | Retention Time |
| SOA | Secondary Organic Aerosol |
| SOZ | Secondary Ozonide |
| TMS | Tetramethylsilane |
| TriMS | Trimethylsilyl |
| VOC | Volatile Organic Compound |

# Chapter 1. Introduction

## *1.1 Importance of Studying Aerosols and Atmospheric Chemistry*

***1.1.1 Large Atmospheric Abundance of Organic and Inorganic Aerosols*** At less than 2.5 microns across, a single aerosol particle is invisible to the naked eye, but when aerosols accumulate in the atmosphere to the concentration 559 $\mu g/m^3$ creating thick smog, they cannot be ignored.[1] The concentration of $PM_{2.5}$ aerosols in Beijing's atmosphere on January 2, 2016 was just that, 22 times the interim level of protection (25 $\mu g/m^3$) set by The World Health Organization.[2] For residents of the city, this is not an oddity, but a normality requiring the use of face masks outdoors, and likely indoors as well. In Beijing and other urban environments, the emission sources of aerosols include vehicle exhaust, fossil fuel combustion, biomass burning, road and soil dusts, cooking, vegetative detritus, and metal processing.[3]

Aerosols are either organic or inorganic particles suspended in the atmosphere. Organic aerosols are carbon-containing compounds emitted particularly through plant processes, biomass burning, and fossil fuel combustion, whereas inorganic aerosols include mineral dusts, soil, and sea salts.[4] Most organic aerosols are formed through atmospheric chemistry of volatile organic compounds (VOCs) (e.g. isoprene and monoterpenes from plants, acetone from paint coatings, and gasoline from fossil fuels), which are gases at room temperature. It is estimated (perhaps underestimated) that there have been up to 100,000 different organic compounds measured in the atmosphere.[5]

VOCs are of particular interest due to their ubiquitous presence in the atmosphere and their impact on climate. Research studying global emissions of gases and aerosols

found that the mean value of VOCs emitted into the atmosphere over a 30-year period from 1980-2010 was 760 Tg/year.[6] It is difficult to imagine a teragram, let alone 760 Tg. This value is equivalent to the mass of over 5 million blue whales (average mass: 150 metric tons) being emitted into the atmosphere every year.[7] The biggest VOC contributor is isoprene, totaling 594 Tg/year. When a compound contains two isoprene units, it is called a monoterpene. Monoterpenes contribute 95 Tg/year. The products of reactions involving VOCs are secondary organic aerosols (SOAs), which are the subjects of numerous atmospheric chemistry studies.

***1.1.2 Aerosols' Impacts on Visibility, Climate, and Health*** The most immediate and noticeable impact of aerosols is the reduction of visibility by scattering light in the atmosphere, resulting in smog and haze. Visibility is the relative ability of an object to be seen via the perceiving of light particles by the eye-brain system. This psychophysical process detects relative differences in brightness, which involves factors such as illumination by the sun, physical characteristics of the object, optical characteristics of atmospheric particulate matter, and the response of the eye-brain system.[8] Aerosols reduce visibility by diffraction, refraction, phase shift, and absorption of particles of light called photons.

Aerosols can directly or indirectly impact climate, which is quantified in terms of aerosols' radiative forcing. Radiative forcing (RF) expressed in Watts/$m^2$ is the net energy change of solar and terrestrial radiation on Earth caused by anthropogenic or natural changes in the atmosphere (e.g. aerosol emissions), Earth's surface, and solar activity.[9] These values enable comparison of climate responses caused by different

atmospheric components. Absorption of terrestrial radiation by greenhouse gases (carbon dioxide, ozone, methane, and nitrous oxide) results in positive RF values which describe a net warming effect.[10] Scattering and reflection of solar radiation by aerosols results in negative RF values which describe a net cooling effect. In 2011, aerosol-radiation interactions were estimated to have an RF of -0.35 Watts/$m^2$ with an error bar of -0.85 to +0.15 Watts/$m^2$ which appears to be net cooling; however the error indicates a possible net warming effect as well.[9] In 2013, the Intergovernmental Panel on Climate Change reported only a medium confidence level in its values reported for total aerosol effect demonstrating the need for further scientific understanding of aerosols.

Aerosols indirectly impact climate via cloud formation by acting as cloud condensation nuclei. Clouds consist of condensed water molecules, which are very small at diameters of 0.00025 μm.[11] Their small size makes it difficult for water molecules to form strong enough interactions to form cloud droplets, instead requiring a surface with a diameter of at least 2 μm on which they can condense.[12] These surfaces are referred to as cloud condensation nuclei (CCN) and can consist of organic and inorganic aerosols. More is known about inorganic aerosols as CCN than organic aerosols. Organic compounds are mostly nonpolar compounds and therefore not typically soluble in water, but some oxidized organics are partially soluble. However, the partially soluble organic aerosol adds solute to the growing water droplet which decreases both its critical supersaturation and surface tension, resulting in accumulation of many smaller droplets as opposed to few larger droplets.[13] The numerous smaller droplets have greater surface area to reflect light, and are therefore whiter. The measure of a cloud's whiteness is cloud

albedo. Greater aerosol concentration means more CCN to seed denser clouds of smaller droplets, and therefore have a higher albedo, reflecting more light back into space, and leaving less energy to heat the Earth's surface resulting in an indirect effect of a global negative RF value (net cooling effect).[13, 14] However, darker organic aerosols, such as brown carbon, absorb radiation resulting in a direct warming effect on the atmosphere. Aerosols can impact climate by cooling and heating; their abundances vary around the planet. Therefore, there is uncertainty about the climate impact of aerosols necessitating more study.

The health hazards of aerosols are due to their small size. With diameters less than 2.5 microns, aerosols can penetrate alveoli of lungs, produce scarring, and cause respiratory and cardiovascular effects, potentially increasing mortality rates.[2, 15] A health impact assessment found that cardiopulmonary mortality in 23 European cities studied could be reduced by over 11,000 deaths if the concentration of $PM_{2.5}$ is reduced to 15 $\mu g/m^3$.[16] Interactions of organic aerosols, nitrogen oxides, and ultraviolet light can reduce visibility by scattering light in the atmosphere during episodes of photochemical smog.[17] Organic compounds that contribute the most to smog formation are terpenes.[18]

***1.1.3 Chemical Modification of Aerosols in the Atmosphere by Ozone*** Although observations of aerosol effects date back at least to the 18$^{th}$ century, there is still much to be studied especially their chemical modification in the atmosphere.[19, 20] Studying how aerosols form, transform, and are removed from the atmosphere will increase scientific understanding of aerosols' environmental effects.[20] Of particular interest to atmospheric aerosol research are aerosol interactions with oxidants such as ozone. Below the

stratosphere, which contains the ozone layer, is the troposphere, the atmospheric layer nearest Earth's surface. The troposphere contains ozone pollution at background concentrations ranging from 35 to 50 ppb in the Northern Hemisphere, with episodes of very high concentrations in urban areas ranging from 200 to 400 ppb.[21] As a highly reactive species, ozone is an effective reagent for cleaving carbon-carbon double bonds (C=C), also called alkene bonds.[22] Alkenes are particularly present in the atmosphere in the form of monoterpenes such as α-terpineol (Figure 1), which is the compound of interest in the present study.

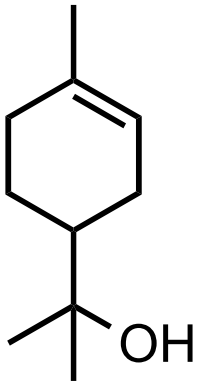


**Figure 1.** Structure of α-terpineol.

This cyclic terpene alcohol can enter the atmosphere directly as an emission from plants, as a component of essential oils such as pine, camphor, neroli, and petitgrain used in household cleaners and perfumes, or as an oxidation product of other monoterpenes such as limonene.[23] Some have described α-terpineol as the most important monocyclic monoterpene alcohol because it can be obtained from other key monoterpenes by simple reactions.

### *1.2 An Introduction to Ozonolysis Chemistry*

***1.2.1 Simple Ozonolysis*** The specific term for ozone's cleaving of C=C bonds, like that of α-terpineol, is ozonolysis.[22] Often the term ozonation is used interchangeably with ozonolysis, but it is a more general term meaning the action of ozone on a substance not specifically on alkenes. The first step of ozonolysis is the 1,3-dipolar cycloaddition of ozone to the unsaturated sites of the C=C bonds, to form a 1,2,3-trioxolane ring, or primary ozonide (POZ), shown in Figure 2.[22, 24] This intermediate species contains the inserted bridge of three O atoms, while retaining the sigma-bond between the C atoms. A cycloaddition is a reaction that joins two π systems of electrons to produce a ring structure.[25] A cycloaddition is a concerted reaction because it occurs in one step as opposed to stepwise addition, in which reactions occur in multiple steps with reactive intermediates. The arrow-pushing mechanism shown in Figure 2 demonstrates the cyclic aspect of the movement of the electrons.

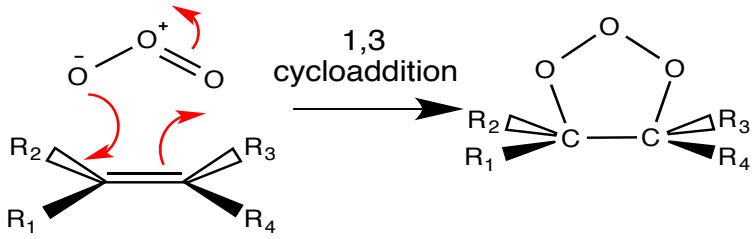


**Figure 2.** Arrow-pushing of electrons in concerted 1,3 cycloaddition step forming primary ozonide (POZ) ring structure.

Computational research studying the reactivity trends of dipolar cycloadditions has compared these mechanisms to stepwise additions, and has found that cycloadditions

have lower energy barriers than stepwise additions with differences in the range of 5-33 kJ/mol.[26]

The favorability of this addition can be understood using frontier molecular orbital (FMO) theory.[26, 27] This theory considers only the the highest occupied molecular orbital (HOMO) and the lowest unoccupied molecular orbital (LUMO) of a reaction. The HOMO acts as a nucleophile while the LUMO acts as an electrophile. In ozonolysis, both species have π systems with ozone having a 4π electron system and the alkene having a 2π electron system.[28] Ozone is an electrophilic 1,3-dipole. The alkene is a dipolarophile. The alkene's HOMO and ozone's LUMO have a small energy gap between them (Figure 3), which makes for a better overlap and interaction of the FMOs which is favorable.[26]

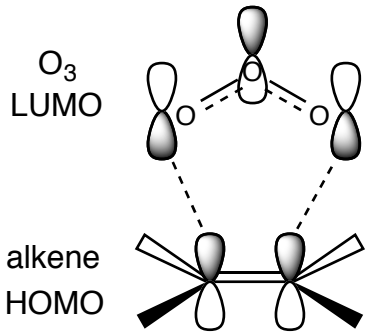


**Figure 3.** Ozone's lowest unoccupied molecular orbital (LUMO) and the alkene's highest occupied molecular orbital (HOMO) overlap beginning the ozonolysis reaction.

The formation of the POZ is highly exothermic (-228 kJ/mol) with the excess energy causing the POZ to collapse rapidly by homolytic cleavage of the C-C bond and one O-O bond in a unimolecular cycloreversion process, also exothermic (-11 kJ/mol).[29] This yields two fragments, one containing a carbonyl bond and the other a carbonyl oxide at the sites of fragmentation (Figure 4).

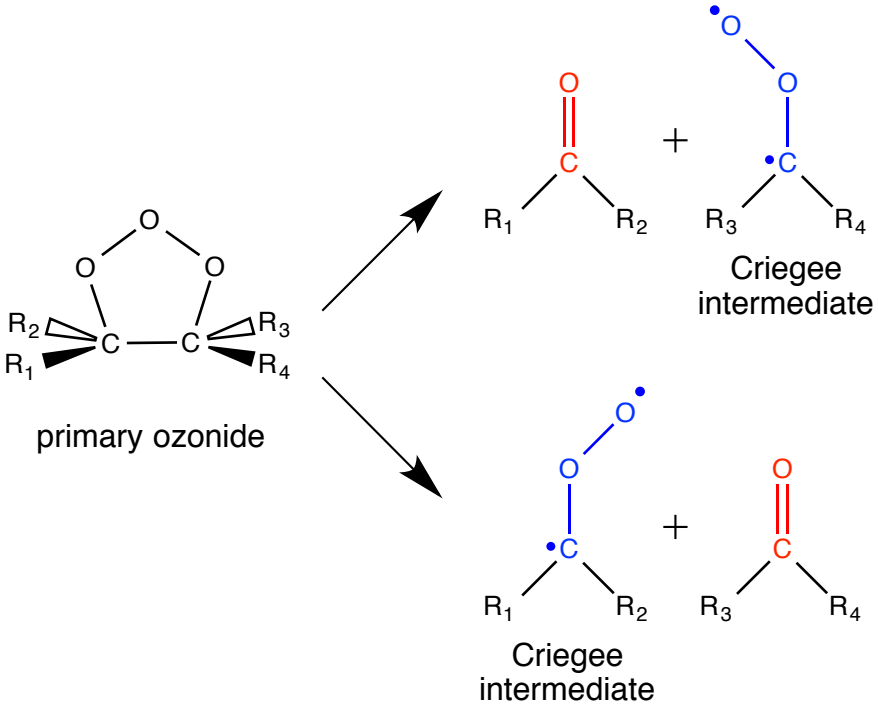


**Figure 4.** The fragmentation of the primary ozonide can yield two different pairs of fragments. Each pair consists of one fragment with a carbonyl and the other with a carbonyl oxide.

Depending on the substituents of the C-C bond and which of the two oxygen-oxygen single bonds (O-O) breaks, two different pairs of fragments can be produced. The carbonyl oxide containing species is a biradical known as the Criegee Intermediate (CI). The identity of this intermediate dates back to 1949 when Rudolph Criegee, an enthusiast

of ozone chemistry, began to study the mechanism of ozonolysis which became known as the Criegee Mechanism.[22]

The post-POZ fragments can then rearrange through an exothermic (-211 kJ/mol) 1,3-cycloaddition process to give 1,2,4-trioxolane, or secondary ozonide (SOZ) shown in Scheme 1.[29]

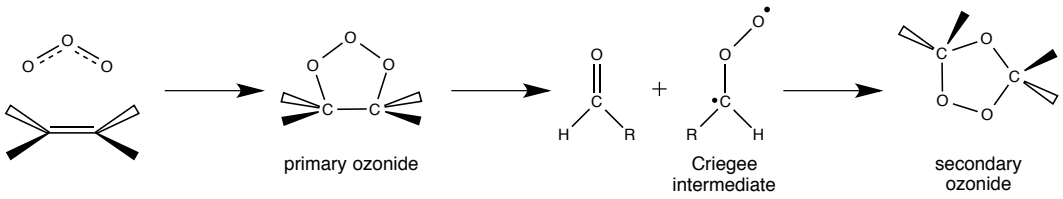


**Scheme 1.** Formation of secondary ozonide.

This product is more stable than previously thought. Although it can and has been isolated, its ring structure is highly strained at low molecular weight causing it to be potentially explosive.[30] SOZs of such monoterpenes as limonene, 3-carene, 4-carene, isolimonene, have been identified using Gas Chromatography/Mass Spectrometry (GCMS) and $^{13}C$ Nuclear Magnetic Resonance Spectroscopy (NMR).[31] The SOZ can then proceed to form further products depending on the presence of oxidative or reductive reagents and the phase of the reaction.

***1.2.2 Organic Ozonolysis Synthesis*** Ozonolysis is a typical process found in organic synthesis literature for its usefulness in cleaving C=C bonds. In organic synthesis, the SOZ leads to formation of aldehydes, ketones, and carboxylic acids, depending on synthetic workup.[32] These workups (Scheme 2) involve either reductive reagents like zinc metal (Zn) in acetic acid ($CH_3COOH$), or sodium iodide (NaI); or oxidative workups like potassium permanganate ($KMnO_4$) in neutral or acidic solution, or

formic acid ($HCO_2H$) and hydrogen peroxide ($H_2O_2$).[32, 33] Reductive workups typically yield products containing aldehydes (R(C=O)H) or ketones (R(C=O)R). Oxidative workups typically yield products containing carboxylic acids ($RCO_2H$). Much recent research involving ozonolysis has not been in organic synthesis, but in atmospheric studies particularly of monoterpenes.

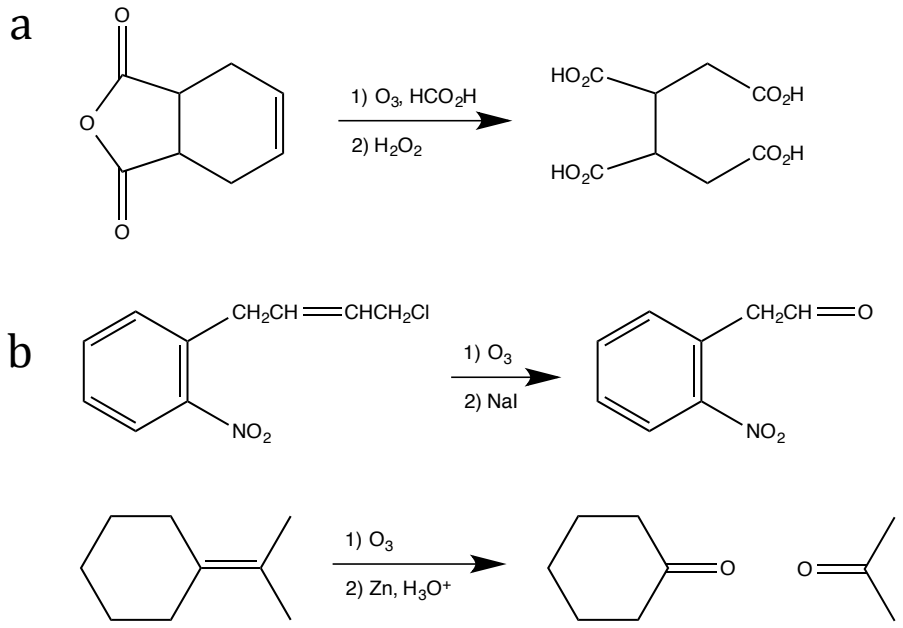


**Scheme 2a.** Oxidative workup.
**Scheme 2b.** Reductive workups.

Ozonolysis in atmospherically relevant phases like gas, heterogeneous, aqueous, and surface-adsorbed differ greatly from organic synthesis. In the atmosphere, oxidative and reductive reagents are not added to workup products. The next section will discuss more specific distinctions between atmospheric and typical organic synthesis.

### *1.3 Atmospheric Ozonolysis Reaction Environments and Their Relevance*

***1.3.1 Gas Phase*** The most studied reaction environment of ozonolysis is the gas phase. In the gas phase, VOCs react with ozone, $NO_3$, and ·OH forming products that are

condensed or dissolved in bulk aerosol phase.[34] The rearrangement of the POZ to form the SOZ is unlikely in the gas phase and instead the POZ will decompose and fragment rapidly.[24] CIs have been indirectly established as a source of free radicals like hydroxyl radicals (·OH) in the atmosphere.[24] For example, the ozonolysis of ethene and terminal alkenes form the CI, $^{\bullet}CH_2OO^{\bullet}$ and stable reaction products including HC(O)H, CO, $CO_2$, $H_2O$ and HC(O)OH by the mechanism shown in Scheme 3.[24]

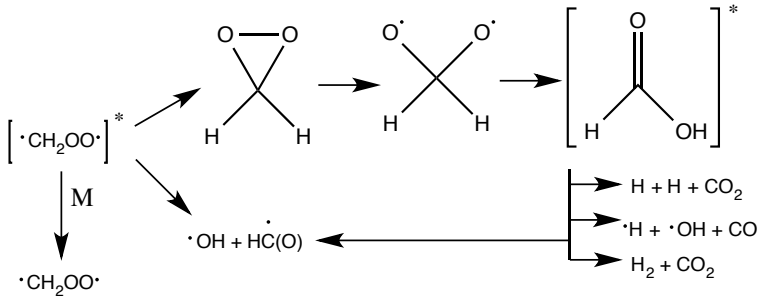


**Scheme 3.** Mechanism of $^{\bullet}CH_2OO^{\bullet}$ decomposition.

These gas-phase products are small due to the fragmentation of the POZ and lack of SOZ formation which would retain larger sizes instead of smaller fragments.[35] However, aqueous ozonolysis mechanisms yield larger products since the SOZ is formed. A comparison of gaseous and aqueous mechanisms is shown in Figure 5.

Studies of the gas-phase ozonolysis of α-terpineol have identified the following products with 33.5% total carbonyl yield using Gas Chromatography/Mass Spectrometry (GCMS) and proposed mechanisms: 2-oxopropanal (major product), ethanedial, 4-methyl-3-cyclohexen-1-one, 6-hydroxy-hept-5-en-2-one, 1,4-butanedial, and 4-oxopentanal (Scheme 4).[36, 37] The first-order reaction rate constant was determined by measuring the decrease in ozone concentration with excess α-terpineol, and was reported to be $3.0 \times 10^{-16}$ $cm^3$ $molecules^{-1}$ $s^{-1}$.[37]

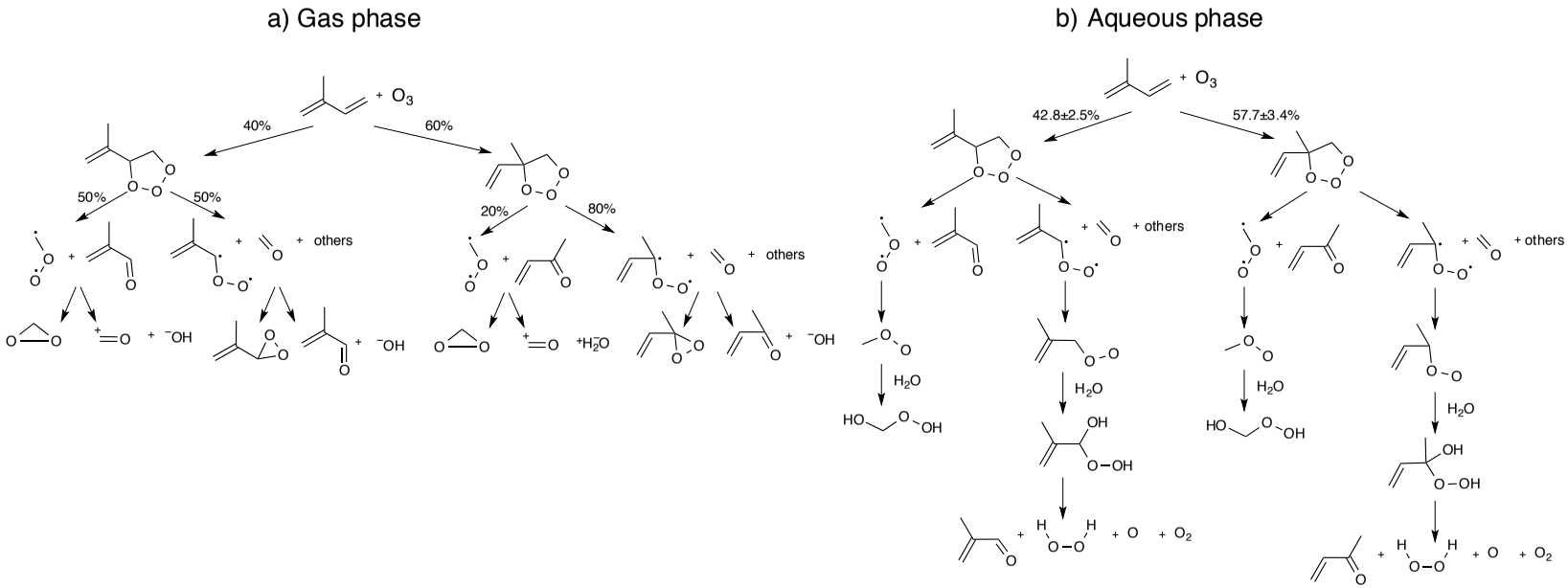


**Figure 5.** Gas phase (a) and aqueous phase (b) mechanisms yield different products. Gas phase products are smaller than aqueous phase products.[35]

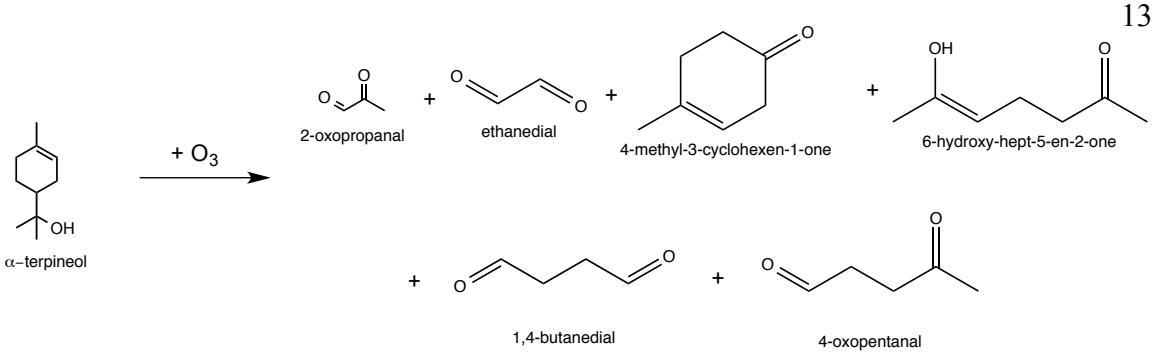


**Scheme 4.** Products of the gas-phase ozonolysis of α-terpineol.

***1.3.2 Aqueous Phase*** Aqueous ozonolysis describes ozonolysis reactions occurring in the presence of water in the aqueous environment. It has been proposed that water can stabilize the energy-rich Criegee radicals resulting in differing total carbon yields for aqueous versus gas-phase ozonolysis of isoprene.[35] It was concluded that gas-phase allows for decomposition, isomerization, stabilization, and bimolecular reactions of the CIs, whereas in aqueous-phase, water stabilizes and reacts bimolecularly with the CIs. Due to the increased presence of water molecules in cloud and fog environments, it is suggested that the increase of water molecules leads to a major increase in CI stabilization and subsequent aqueous-phase product formation.[38]

***1.3.3 Heterogeneous Phase*** The term heterogeneous describes reactions in which the reactants are not in the same phase. This includes reactions between gases and liquids, gases and solids, solids and liquids, and surface-adsorbed reactions. Most atmospheric studies of heterogeneous reactions involve the surface-adsorbed reaction. Surface-adsorbed describes reactions in which one reactant (adsorbate) is adsorbed onto a material (adsorbent) creating a thin film prior to being exposed to another reactant, typically a gaseous flow. An example mechanism of catechol heterogeneous ozonolysis is shown in Scheme 5.[39]

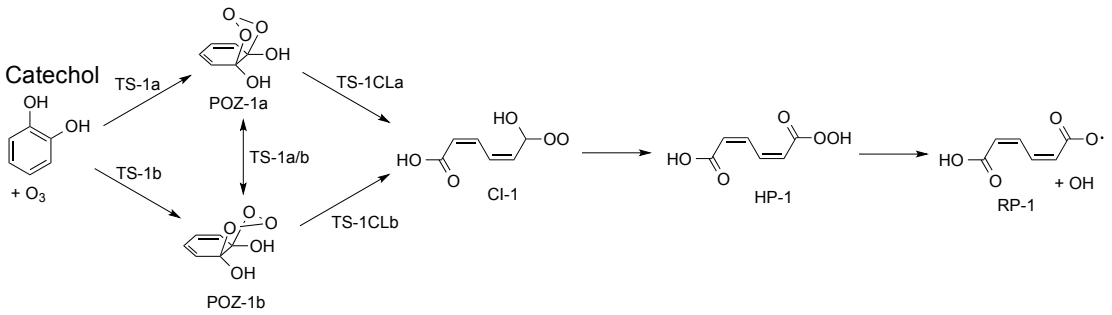


**Scheme 5.** Ozonolysis of catechol.[39]

Research has shown that heterogeneous ozonolysis of organic compounds proceed at faster rates than their homogeneous gaseous counterparts.[39, 40] Several studies have focused on the fate of semi-volatile organic pesticides in the atmosphere. One group of researchers compared their own data of three different pesticides adsorbed on quartz to seven other adsorbates on six different adsorbents.[41] They found that ozone reactivities depend on both the structure of the adsorbate and the material serving as the adsorbent. The researchers determined the tropospheric lifetimes of the pesticides based on their reactivities toward ozone, finding they ranged from 5 min. for benzo[a]pyrene on soot to 12 months for folpet (2-(trichloromethylsulfanyl)isoindole-1,3-dione) on quartz plaques, with most adsorbate/adsorbent combinations providing half lives longer than one week. The longer lifetimes led the researchers to suggest that the pesticides can be transported to regions away from their application site.

Other atmospheric heterogeneous reaction studies focus on ozonolysis of biogenic VOCs such as isoprene and monoterpenes. One study found that isoprene's oxidation products, methacrolein and methyl vinyl ketone yielded a greater amount of products in a heterogeneous reaction (adsorbed on silica ($SiO_2$)) than in a homogeneous gaseous reaction, suggesting that the heterogeneous reaction is competitive with the homogeneous reaction.[42]

The surface reaction of ozone and α-terpineol adsorbed on beads of three typical indoor surfaces, glass, polyvinyl chloride (PVC), and latex paint has been studied to determine the effect of relative humidity on these reactions.[43] The presence of water was found to have the greatest affect on glass surfaces. Relative humidity changed the adsorptive capacity, but made little impact on the second-order reaction rate constant, $k_2$, and ozone reactivity was dependent on the interfacial activity of α-terpineol. This study compared surface ozonolysis of α-terpineol to gas-phase ozonolysis, and found reaction probabilities on surfaces to be larger. The rate constant, $k_2$, for the surfaces studied were found to be in the range of (2-15) x $10^{-16}$ $cm^3$ $molecule^{-1}$ $s^{-1}$.

***1.3.4 Present Research*** Several atmospheric chemistry studies have focused on gas-phase ozonolysis, and consequently, there is little known about aqueous-phase reactivity. The present research seeks to understand the aqueous ozonolysis of α-terpineol, both its products and mechanism, using one- and two-dimensional Nuclear Magnetic Resonance (NMR) Spectroscopy and Gas Chromatography/Mass Spectrometry (GCMS) techniques to monitor the reaction and identify its products. Defining the phase of this reaction is more complex than in simple aqueous solution because gaseous ozone is used, and ozonolysis can occur in solution near the surface, in the bulk of the solution, or at the interface. Recent reports suggest that surface or interfacial reactions may be more significant than bulk-phase reactions.[38] The aqueous droplet reaction environment is modeled in Figure 6.

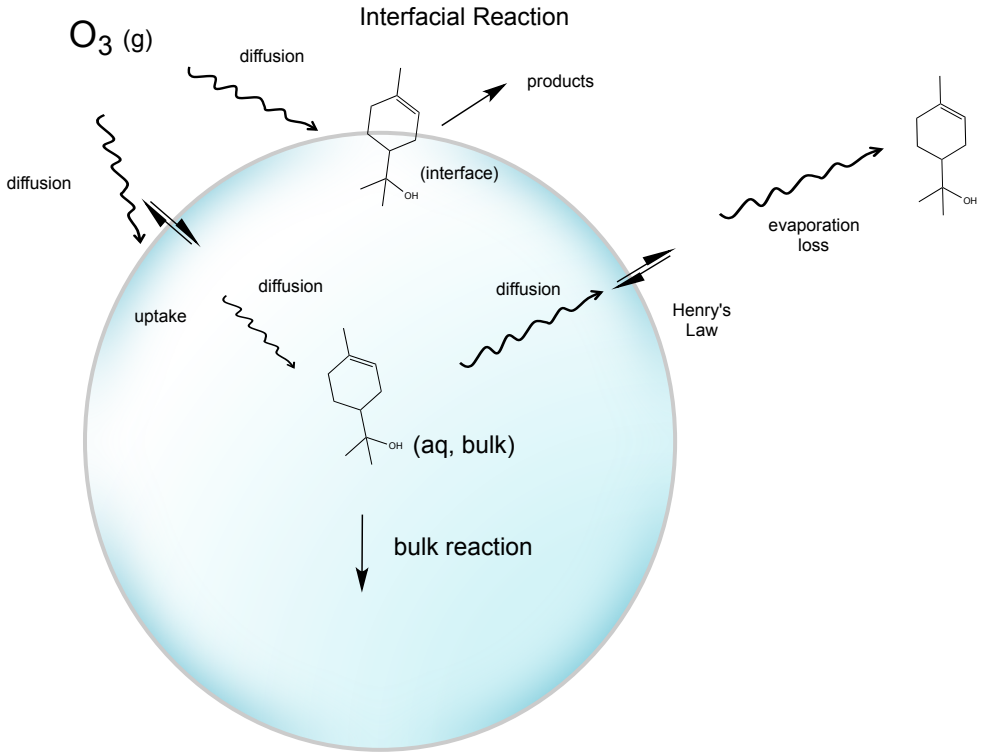


**Figure 6.** The aqueous environment, such as in cloud droplets, is an unusual medium for ozonolysis, as it differs from both organic synthesis and gas phase. The reaction may take place in the bulk of the droplet or at the interface.

Although uncommon, NMR spectroscopy has been used for structural analysis of organic aerosol experiments.[44] NMR experiments, both 1-D ($^1$H) and 2-D (COSY and HSQC), have been used to identify limonene SOA functionalities in a mixture of multifunctional compounds that were difficult to isolate. Abundance of the different functionalities has been quantified using ratios of integrated signals of different functionality regions. The ozonolysis of aqueous α-terpineol may contribute to the formation of secondary organic matter in cloud droplets. This research seeks to better understand the role of aqueous chemistry in the atmosphere, its kinetics, mechanism, and atmospheric impact in comparison to the much-studied gas chemistry in the atmosphere.

# Chapter 2. Methods

## *2.1 Ozonolysis Reaction*

***2.1.1 Reaction Preparation*** A saturated solution (~6 mL, ~3mM) of α-terpineol was prepared by sonicating excess α-terpineol in deuterated water for 10 min. Tetramethylammonium chloride ($N(CH_3)_4Cl$, 0.05g) was then added to 5 mL of the solution for a final concentration of 91 mM. Tetramethylammonium chloride was chosen as the internal standard because it is nonvolatile, does not react with the starting materials, and its $^1H$ NMR peak does not overlap with that of the reactants and products. The experiment was conducted in a 1-L round-bottom flask attached to a rotor (Buchi RE 111) spinning at maximum speed to create a thin film on the inner surface of the glass with a surface area of 265 $cm^2$. The reaction set up is shown in Figure 7.

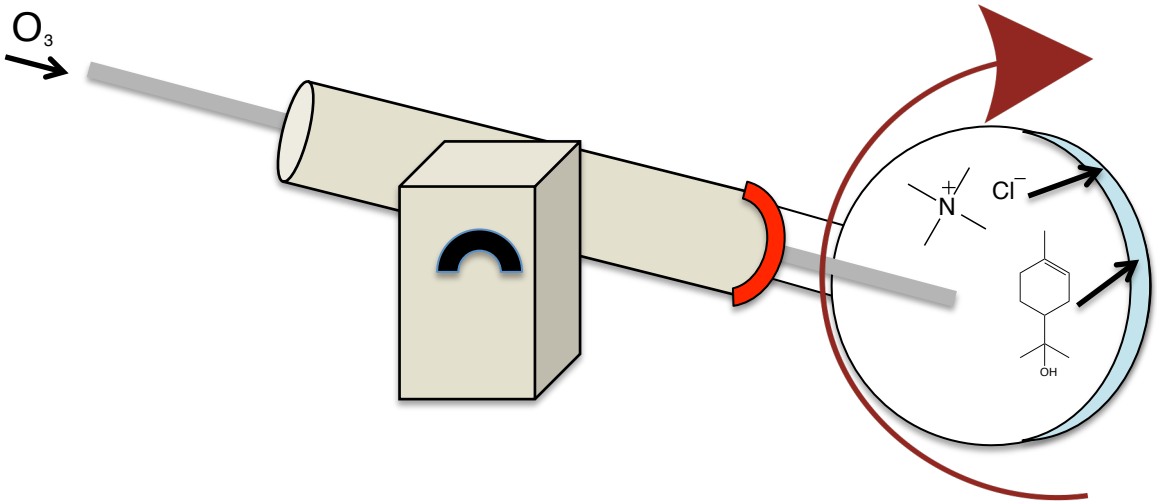


**Figure 7.** Reaction set up includes a rotating round-bottom flask, which creates a thin film of the aqueous α-terpineol solution containing tetramethylammonium chloride as the internal standard, and air mixed with ozone flowing into the flask.

Ozone was produced by a photolytic ozone generator (Jelight 600). It was mixed with air and allowed to flow into the flask. Ozone and air flow rates were monitored with flow meters (Matheson 600 E100) and held relatively constant at a combined flow rate

which varied from 56.53 to 60.46 sccm. Separate experiments were conducted with varying ozone concentrations (approximately 131, 480, and 965 ppb) which were measured with an ozone monitor (Jelight 465L) before the reaction. Additional variables were studied, including acidifying the environment by adding sulfuric acid (5 μL, 0.10 M) and changing the solvent to methanol. Acidifying the solution did not impact the results. Changing the solvent to methanol did not yield a reaction between ozone and α-terpineol.

***2.1.2 Reaction Monitoring and Product Extraction*** $^{1}$H NMR spectra were taken of the α-terpineol solution before the reaction and at 30 and 60-min intervals until reaction completion, which ranged from six to twenty-four hours, depending on $O_3$ concentration. Products were extracted into deuterated chloroform ($CDCl_3$) using a separatory funnel and concentrated with a gentle flow of nitrogen gas. The concentrated, extracted products were analyzed with $^{1}$H, $^{13}$C, COSY, and HSQC NMR, GCMS, and Attenuated Total Reflectance-Fourier Transform Infrared Spectroscopy (ATR-FTIR). NMR is a non-destructive technique, whereas GCMS and ATR-FTIR are destructive techniques.

### *2.2 Product Identification*

***2.2.1 One-Dimensional Nuclear Magnetic Resonance Spectroscopy*** By exploiting the magnetic properties of atomic nuclei, Nuclear Magnetic Resonance Spectroscopy (NMR) provides structural information about organic molecules. The nucleus of an atom carries a positive charge because it consists of positively charged protons and neutral neutrons. The “spinning” of positively charged nuclei having either

an odd atomic number or odd atomic mass generates a magnetic field with a magnetic moment μ, as shown in Figure 8.[45]

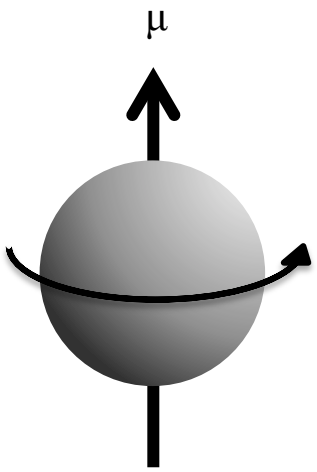


**Figure 8.** A spinning nucleus generates a magnetic field with a magnetic moment, μ.[45]

Organic molecules contain the common atoms carbon, hydrogen, oxygen, nitrogen, phosphorus, and fluorine. All of these except oxygen have isotopes meeting the odd atomic number criteria, such that $^{1}H$ and $^{13}C$ have a spin magnetic moment, which can be either +½ or -½, but $^{12}C$ and $^{16}O$ do not. The spinning nuclei have a non-zero spin quantum number, *I*. Isotopic nuclei with $I = ½$ are the predominant type of nuclei studied using NMR.

NMR is based on the principle that molecular structure can be elucidated based on how the structural arrangement of atoms affects nuclear magnetic properties. The experiment involves applying a strong, superconducting external magnetic field to nuclei of magnetic isotopes such as $^{1}H$ and $^{13}C$ by placing the nuclei between poles of the magnet. Prior to experiencing the applied magnetic field, the nuclei have random orientation and two spin states, +½ and -½, of degenerate (equal) energy. When

experiencing the applied magnetic field $\beta_o$, the spins of the nuclei can become aligned with the magnetic field, which is the low-energy state, or against the magnetic field, which is the high-energy state. The splitting of the two states into different energies is called the Zeeman effect.[45]

Energy is pulsed on the order of microseconds to excite the nuclei from the low-energy state to a high-energy state. Between pulses, the nuclei relax back to the low-energy state. During this relaxation, the nuclei release radiation (Figure 9), which is described on the free induction decay (FID) within a time domain. To obtain the frequency domain spectrum, the FID signal is Fourier transformed to a spectrum with frequency and concentration domains.

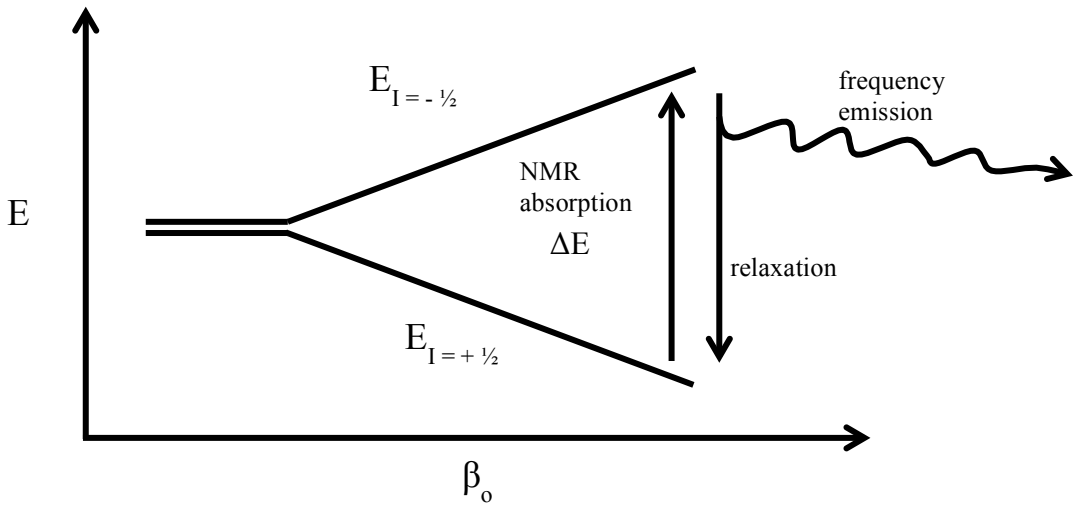


**Figure 9.** When a magnetic field is applied, an energy gap exists between the spin states. A nuclei relaxing from high to low energy emits energy at a specific frequency but is usually accomplished by non-radiative processes.

The radiation absorbed is characteristic of different nuclei according to the specific electron density surrounding those nuclei, which varies depending on the neighboring atoms. The effective magnetic field a nucleus experiences is not equal to the

applied magnetic field; it depends on the surrounding atoms and their electron density because electron density shields the nucleus from the applied magnetic field. A nucleus experiencing more of the magnetic field is described as deshielded, while a nucleus experiencing less of the magnetic field is described as shielded. Shielding and deshielding affect the frequency absorbed, and the variation of the frequency is referred to as chemical shift, in units of ppm.

Close proximity to single atoms or groups of atoms that remove electron density will deshield a nucleus, resulting in a higher frequency and chemical shift. An example of a group of atoms with this effect is the aldehyde, which contains a carbonyl (carbon-oxygen double bond). Oxygen is more electronegative than carbon, so it will draw electron density away from carbon. This in turn draws electron density away from the proton bonded to the carbon, which makes the carbonyl an electron-withdrawing group. This exposes the proton's nucleus to more of the applied magnetic field, resulting in a high chemical shift for the aldehydic proton in the 9-10 ppm range. A proton on an alkane chain is well shielded because the surrounding atoms (carbon and hydrogen) do not greatly withdraw electron density from the given proton. Therefore, the proton experiences less of the magnetic field, resulting in a low chemical shift in the 0-2 ppm range.

Chemical shifts are also affected by pi bonds. This type of bonding is present in multiple bonds, such as the double bond of alkenes (C=C). This bond consists of a sigma bond composed of overlapping hybridized orbitals and a pi bond composed of overlapping p orbitals. The electrons of the pi bond circulate, which induces a local

magnetic field. This induced magnetic field exists in the same direction as the applied magnetic field of the NMR's magnet, reinforcing the field experienced by the proton, which deshields the nucleus of the proton. This results in a higher chemical shift for alkene protons in the 4-6 ppm range, as compared to alkane protons in the 0-2 ppm range.

Comparing an experimental chemical shift to typical ranges of alkanes, alkenes, aromatics, carbonyls, alcohols, ethers, esters, amines, etc. can elucidate the structural elements of a molecule. Tables 1 and 2 report typical NMR proton and carbon chemical shifts, respectively. The molecule tetramethylsilane (TMS) (Figure 10) is used as a reference in NMR because few protons are more shielded than those of TMS. Therefore, the chemical shift of the protons of TMS is assigned the value of 0 ppm. Proton chemical shifts are given values based on how deshielded they are compared to the protons of TMS.

**Table 1.** Proton chemical shifts.

| **Functionality** | **Approximate Chemical Shift Range (ppm)** |
|---|---|
| alkane | 0.2-2.0 |
| alkene | 4.5-6.2 |
| alkyne | 1.5-3.7 |
| aromatic | 6.4-8.2 |
| ketone | 2-2.5 |
| alcohol | 3.3-4.1 |
| ether | 3.1-3.9 |
| ester | 3.5-4.3 |
| amine | 2.5-3.1 |
| aldehyde | 9.7-10.3 |

**Table 2.** Carbon chemical shifts.

| **Functionality** | **Approximate Chemical Shift Range (ppm)** |
|---|---|
| alkane | -2-45 |
| saturated alkene | 110-160 |
| disubstituted alkene | 140-160 |
| alkyne | 65-80 |
| aromatic | 110-160 |
| ketone | 195-215 |
| alcohol | 50-75 |
| ether | 60-80 |
| ester | 160-175 |
| amine | 25-65 |
| aldehyde | 190-205 |

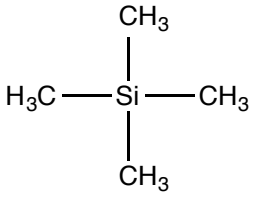

**Figure 10.** All 12 protons of tetramethylsilane have a chemical shift of 0 ppm.

Just as neighboring proton nuclei affect the chemical shift of a proton, the neighbors also affect a proton's signal by splitting it, making one spin state more favored than the other. This effect, called spin-spin splitting or indirect coupling, occurs because the spin of a nucleus polarizes surrounding electrons slightly which in turn polarizes the electrons of a neighboring atom, which polarize that atom's nucleus, splitting the signal into the two spin states.[45] The splitting of a signal is quantified as multiplicity. A proton without neighboring nuclei has a signal that is not split, thus the multiplicity is 1 and a singlet splitting pattern results. A proton with one neighbor has a signal with two peaks, thus a multiplicity of two and a doublet splitting pattern results. Table 3 describes further multiplicities.

**Table 3.** The splitting pattern of a nucleus's signal is dependent on its number of neighboring nuclei.

| **Number of Neighboring Nuclei n** | **Multiplicity n + 1** | **Splitting Pattern** |
|---|---|---|
| 0 | 1 | singlet |
| 1 | 2 | doublet |
| 2 | 3 | triplet |
| 3 | 4 | quartet |
| 4+ | 5+ | multiplet |

Neighboring nuclei within two bonds from each other (vicinal) are said to be coupled to each other. The peak intensities are specific to the splitting pattern and follow

the binomial expansion of coefficients in Pascal's triangle (Figure 11). The numbers of each symmetric row correspond to the ratio of peak intensities. For example, a proton with two neighbors will have triplet splitting pattern. The middle peak in the triplet signal will be the tallest and the peaks on either side will be half the height of the middle peak. Figure 12 shows how the splitting patterns appear in a NMR spectrum.

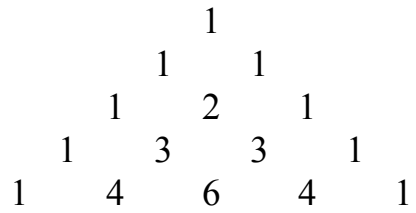


**Figure 11.** Pascal's triangle. Each row is symmetric and the numbers correspond to a ratio of a signal's peak intensities.

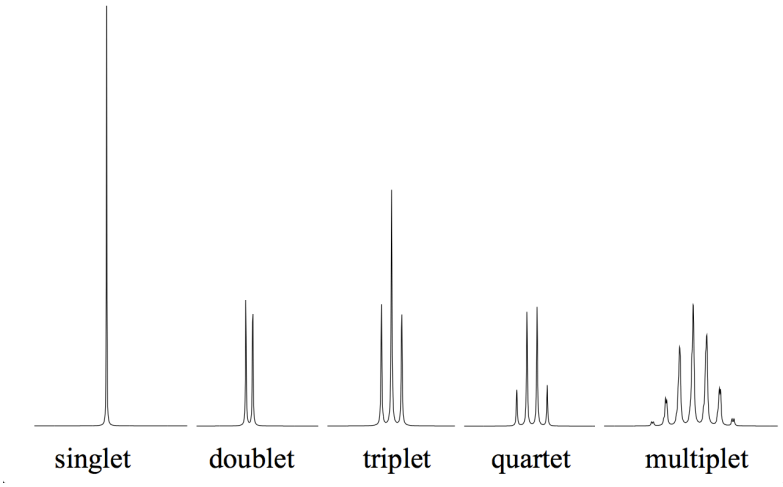


**Figure 12.** Splitting patterns of nuclei.

The difference in frequency of the peaks in a signal is called J coupling and can provide information about the angle between a specific proton and its neighbors. When looking straight on at a carbon atom, the angle between protons on each carbon is called the dihedral angle, Φ (Figure 13).

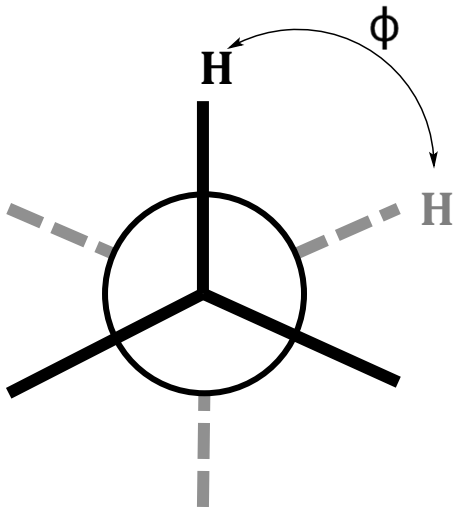


**Figure 13.** The angle between nuclei three bonds away from each other is the dihedral angle.

The Karplus equation (Equation 1) describes the relationship between the dihedral angle and J coupling values.[45]

$$J=\begin{cases} A\cos^2\phi+C & (\phi=0\text{-}90°) \\ A'\cos^2\phi+C' & (\phi=90\text{-}180°) \end{cases} \quad \text{(Equation 1)}$$

Constants vary depending on the system, but C and C' are usually less than 0.3Hz and A and A' are 8-14Hz with A less than A'. The graph shown in Figure 14 demonstrates the J value as a function of the dihedral angle in the Karp lus equation. Maxima lie at angles nearing 0˚ and 180˚, and the minima lies at angles nearing 90˚.

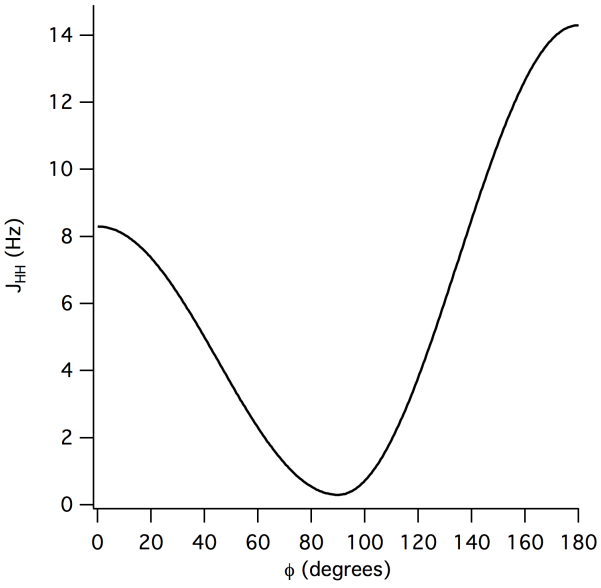


**Figure 14.** The Karplus equation as a function of the dihedral angle.

NMR solvents are deuterated in order to lock the signal of the sample and to ensure they do not interfere with the $^{1}H$ signal of the compound. The signal can drift which requires locking of a nucleus that will not be observed or decoupled. Since $^{1}H$ is being observed, another candidate to l ock onto is deuterium ($^{2}H$), a heavy isotope of hydrogen, which contains a proton and a neutron in its nucleus instead of just a proton like hydrogen. Solvents like water, chloroform, and methanol are deuterated by replacing all of their hydrogen atoms with deuterium atoms. The NMR instrument locks to the $^{2}H$ signal of the solvent. The present research studies aqueous ozonolysis, therefore water would be the desired reaction solvent, but deuterium oxide (deuterated water) is used instead in order to study the reaction progress with NMR.

$^{1}H$ and $^{13}C$ NMR spectra are referred to as one-dimensional. The x- and y-axes display frequency (chemical shift) and intensity, respectively. For $^{1}H$ NMR, the integrated area under a peak is called integration and proportionally corresponds to the

number of protons of that type. The ratio of integrations describes the ratio of proton types in a molecule. The $^{1}H$ and $^{13}C$ NMR spectra of α-terpineol are shown in Figures 15 and 16, respectively, as examples.

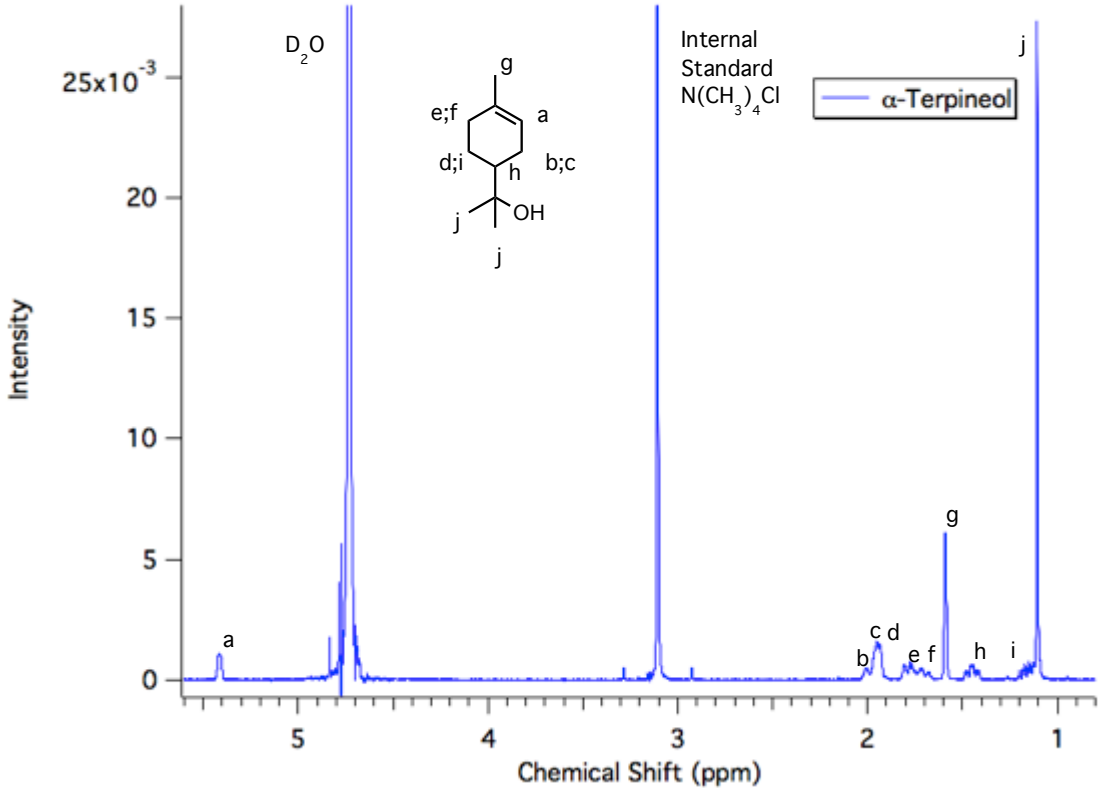


**Figure 15.** Labeled proton NMR spectrum of α-terpineol.

In the $^{1}H$ spectrum of α-terpineol, the solvent and internal standard have chemical shifts of 4.7 ppm and 3.1 ppm, respectively. All chemical shifts and integrations are reported in Table 4. The integration values are relative to the integration of peak b, which had the smallest integration and corresponds to a single proton in α-terpineol. The most intense α-terpineol peak is labeled "j" and corresponds to the six identical protons of the two methyl groups near the alcohol with a chemical shift of 1.1 ppm and a relative integration of 6.9746. It has a singlet splitting pattern because it does not have any non-

identical neighboring nuclei. The proton on the double bond corresponds to the peak labeled “a” which has the highest chemical shift (5.4 ppm) because this proton is the most deshielded. Peak “a” has a relative integration of 1.1036, consistent with its corresponding to a single proton. Protons on the ring have many neighboring nuclei coupled to them and varying dihedral angles, so their splitting patterns are very complicated as demonstrated by peaks b, c, d, e, f, h, and i.

**Table 4.** Chemical shifts and integrations of $^{1}$H NMR spectrum α-terpineol.

| Proton | Chemical Shift (ppm) | Integration |
|---|---|---|
| a | 5.14 | 1.1036 |
| b | 2.01 | 1.0000 |
| c | 1.95 | 1.0595 |
| d | 1.93 | 1.1167 |
| e | 1.79 | 1.2613 |
| f | 1.69 | 1.0799 |
| g | 1.59 | 3.3723 |
| h | 1.44 | 1.1669 |
| i | 1.14 | 1.1207 |
| j | 1.10 | 6.9746 |

In the $^{13}$C spectrum of α-terpineol (Figure 16), the solvent does not have a signal since it does not contain any carbons. Carbons labeled “a” and “b” have the highest chemical shifts (135.9 and 120.8 ppm, respectively) as they are alkenes. The remaining carbons on the ring (d, e, g, h) have lower chemical shifts (44.3, 30.4, 24.9, and 23.6 ppm, respectively) because they are saturated alkanes. This holds for the other saturated carbons (f and i) as well. The carbon labeled “c” only has single bonds, but it is not saturated with protons, so it has a higher chemical shift than the saturated carbons (d-i).

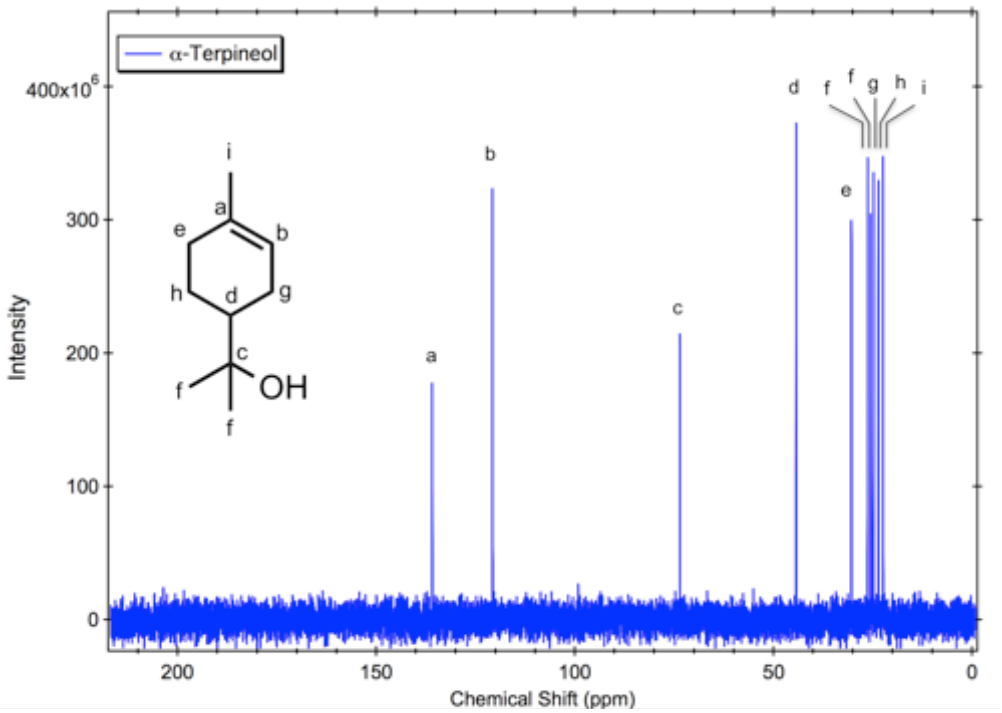


**Figure 16.** Labeled carbon NMR spectrum of α-terpineol.

Characteristic NMR assignments of products were verified using theoretical NMR calculations computed in Gaussian.[46] The theoretical calculations used the gauge-independent atomic orbital (GIAO) method, which is a preferred method for reliable results.[47] Structures for α-terpineol, secondary ozonide, lactone, and cis and trans lactol isomers were optimized with the B3LYP function using the 6-311++G(d,p) basis set. The optimized structures were then optimized to consider the effect of the solvent, water, by using the default solvation model, the Polarizable Continuum Model (PCM), which uses overlapping spheres to create the solute cavity within the solvent. Following optimization with solvation, theoretical NMR data were obtained by computing coupling constants (J values) and chemical shifts. The method used to calculate the coupling constants was

spin-spin mixed. The theoretical coupling constants were used to generate theoretical $^1$H NMR spectra for individual signals as Lorentzian functions

$$L(x)=\frac{1}{\pi}\frac{\Gamma}{(x-x_0)^2+\Gamma^2} \qquad \text{(Equation 2)}$$

where $L$ is the intensity, $\Gamma$ is the half-width of the signal, $x$ is the chemical shift, and $x_0$ is the center of the signal. Half-widths were arbitrarily assigned to match experimental half-widths. The theoretical proton $^1$H NMR spectra were generated using the theoretical and experimental centers and compared to experimental spectra.

***2.2.2 Two-Dimensional Nuclear Magnetic Resonance Spectroscopy*** Other NMR experiments add a second frequency domain, which can provide information about how nuclei correlate through connectivity or space.[45] These NMR spectra are referred to as two-dimensional because they have two frequency domains. These spectra are generated by pulsing the sample twice instead of once. Data is acquired during the second pulse. For one spectrum, multiple experiments are conducted by varying the length of time for the first pulse.[48] The FID of the second time domain is Fourier transformed, followed by the first time domain. This generates a contour plot. When both axes of the plot have the same nuclei (homonuclear), the contours on the diagonal are the one-dimensional spectrum, and any contours off the diagonal represent correlations between nuclei. The diagonal contours represent the one-dimensional spectrum since the identical nuclei will always correlate. When the axes of the plot have different nuclei (heteronuclear), all contours represent correlations between nuclei. The two types of two-dimensional NMR used in the present study are Correlation Spectroscopy (COSY) and Heteronuclear Single Quantum Correlation (HSQC). The contours of the COSY plot

demonstrate correlations between proton nuclei that are within three bonds of each other. The contours of the HSQC plot demonstrate correlations between proton nuclei and the carbon nuclei to which they are bonded. The COSY and HSQC contour plots of α-terpineol are shown in Figures 17 and 18, respectively, as examples.

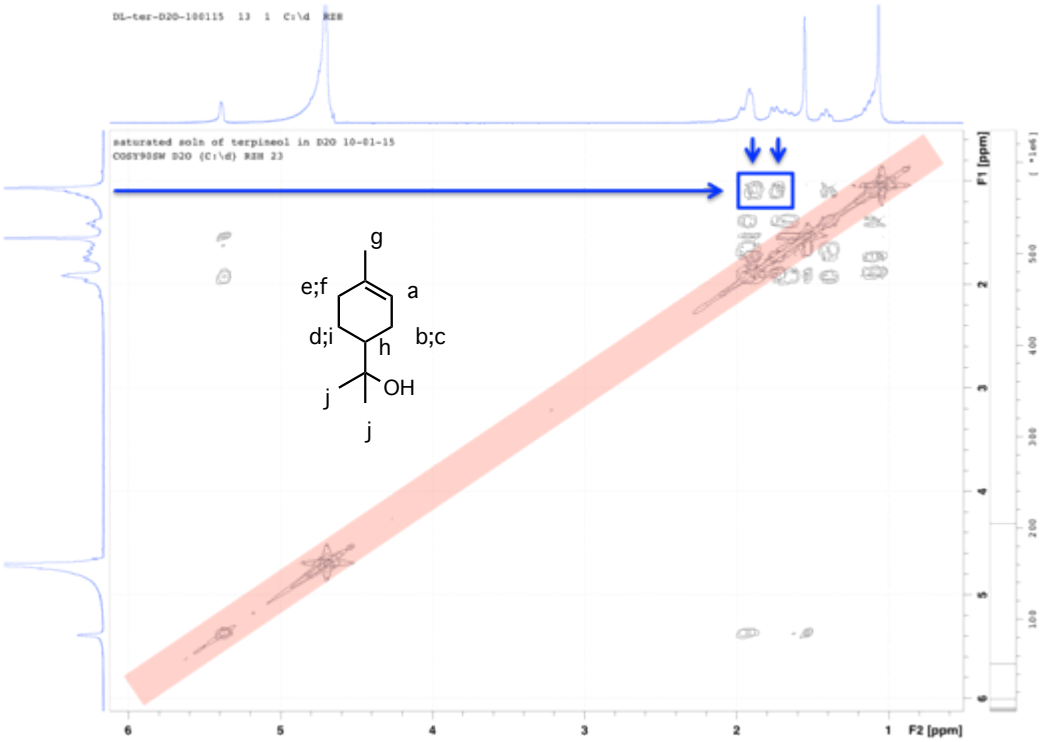


**Figure 17.** COSY NMR spectrum of α-terpineol. The light red highlighted box is the diagonal representing the one-dimensional proton spectrum. The blue box shows an example of off-diagonal contours.

In the COSY spectrum of α-terpineol, the diagonal is highlighted in light red and corresponds to the $^{1}$H NMR spectrum. Visually it appears as a bird's eye view of the spectrum. Identical nuclei have contours that make up the diagonal. For example, 1.5 ppm on the x and y axes has a contour. Off-diagonal contours are correlations between non-identical proton nuclei within three bonds of each other. For example, the contours in

the blue box show correlations between the 1.0 ppm signal and both the 1.7 and 1.9 ppm signals. These correlations agree with the assignments made on the proton spectrum (Figure 15) suggesting these contours are the correlations between proton “i” and protons “c” and “d.”

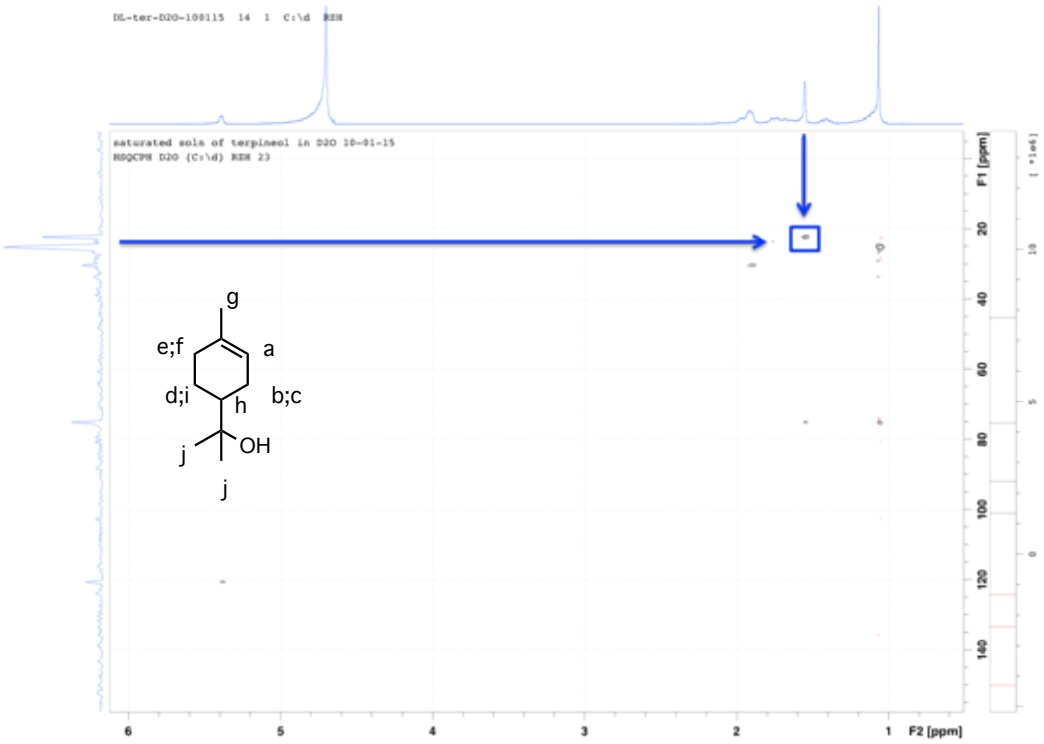


**Figure 18.** HSQC NMR spectrum of α-terpineol. The 1H spectrum is plotted on the x-axis. The 13C spectrum is plotted on the y-axis. The blue box shows an example of a correlation between a proton nucleus (1.6 ppm) and a carbon nucleus (25 ppm).

In the HSQC spectrum of α-terpineol, there is no set of diagonal contours. Contours shown are correlations between proton nuclei and carbon nuclei. For example, the contour in the blue box show correlations between the 1.6 ppm proton signal and the 25 ppm carbon signal. These correlations agree with the assignments made on the proton

(Figure 15) and carbon (Figure 16) spectra suggesting these contours are the correlations between proton “g” and carbon “i.”

***2.2.3 NMR Instrument Parameters and Methods*** NMR spectra were obtained using a Bruker 400MHz NMR - ICON-NMR (Automation). All NMR experiments were conducted in 5 mm NMR tubes. Spectra were taken with deuterated water or deuterated chloroform as the solvent. α-Terpineol and its ozonolysis products are not very soluble in water; therefore, spectra were taken with greater than standard number of scans. $^{1}H$ spectra were taken with 64 scans; $^{13}C$ with 16384 scans; COSY with 64 scans; and HSQC with 256 scans. One-dimensional spectra were analyzed in Igor.

***2.2.4 Gas Chromatography/Mass Spectrometry*** A popular analytical technique for identifying the structures of components in a mixture of organic volatile or semi-volatile compounds is Gas Chromatography/Mass Spectrometry (GCMS). This instrument combines two techniques to first separate component molecules in a mixture and second to ionize these components to determine their masses and predict their structures. The instrument predicts structures by comparing mass spectra of the samples’ components to standard mass spectra from the National Institute of Standards and Technology (NIST) library. The probability of the accuracy of these predictions is also reported.

In the present research, GCMS was utilized to determine the amount and molecular weights of major and minor compounds in the product mixture, to approximate the product ratios, and to identify the presence of alcohol groups in any products by derivatization. The experiments were carried out on an Agilent 7890 Gas Chromatograph

and an Agilent 5975 Mass Selective Detector. Injections (1 μL) were introduced to an SLB-5ms column (30 m × 250 μm, 0.25 μm, Supelco 28471-U) with a pulsed split inlet, split ratio of 10:1, and split flow of 12 mL/min. The oven was set to an initial temperature of 75˚C for 5 min., followed by a temperature ramp of 4˚C/min. to 120˚C for 2 min., then 15˚C/min. to 200˚C for 5 min., and 15˚C/min to 230˚C for 1 min, for a total run time of 31.583 min. The ion scan range was wide from m/z = 15 to m/z = 350. Products were derivatized with BSTFA (N,O-bis(trimethylsilyl) trifluoroacetamide)/10% TMCS (trimethylchlorosilane) reagent. The BSTFA reagent replaces the H of any alcohol group with a trimethylsilyl (TriMS) group.[49] TriMS groups are very polarizable which increases the ionization intensity in the GCMS, which enables determination of alcohol groups depending on how many TriMS groups are present.

***2.2.5 Infrared Spectroscopy*** An analytical technique to identify types of bonds and functional groups present in molecules is Infrared Spectroscopy (IR), which looks at molecular vibrations characteristic of different bonds. In the present research, IR was conducted with an attenuated total reflection crystal (IR-ATR) to verify the presence of carbonyls, which have a strong characteristic peak near 1690-1760 $cm^{-1}$. The experiments were carried out on a Nicolet iS10 with FT-IR ATR accessory. The spectra were acquired as absorbance over the wavenumber range of 728-4000 $cm^{-1}$ with 4 $cm^{-1}$ resolution and 64 scans. Samples for IR-ATR were prepared by concentrating the sample in chloroform with a gentle flow of nitrogen gas. A drop of the concentrated sample was placed on the crystal and the solvent was allowed to evaporate for two minutes before acquiring the spectrum. An inverted funnel with nitrogen gas flowing through it was placed over the

crystal to ensure all solvent was evaporated and only the desired compound remained on the crystal. This process was repeated until the spectrum absorbances did not change, which typically was after three or four drops.

# Chapter 3. Results and Discussion

## *3.1 Reaction Progress and Formation of Products*

Gaseous ozone and aqueous α-terpineol reacted to completion in approximately 10 hours, as monitored by $^{1}$H NMR. After 10 hours, no change was observed in $^{1}$H NMR. The initial terpineol $^{1}$H NMR spectrum overlaid with the final product spectrum show clearly that terpineol peaks disappear and distinct product peaks have grown in (Figure 19). Each spectrum was normalized to the constant concentration of the internal standard, tetramethyl ammonium chloride (Figure 20).

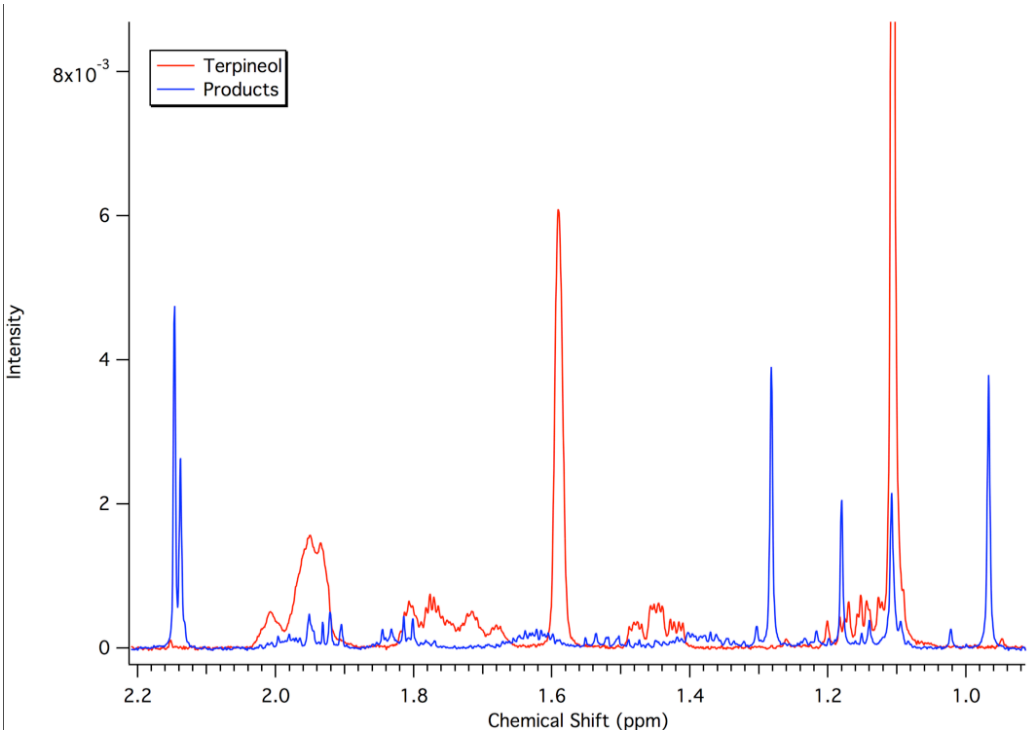


**Figure 19.** Over the chemical shift range of 0.92 to 2.2 ppm), the initial terpineol $^{1}$H NMR spectrum overlaid with the final product spectrum demonstrate that terpineol peaks disappear (e.g. 1.58 ppm) and distinct product peaks have grown in (e.g. 1.28 ppm).

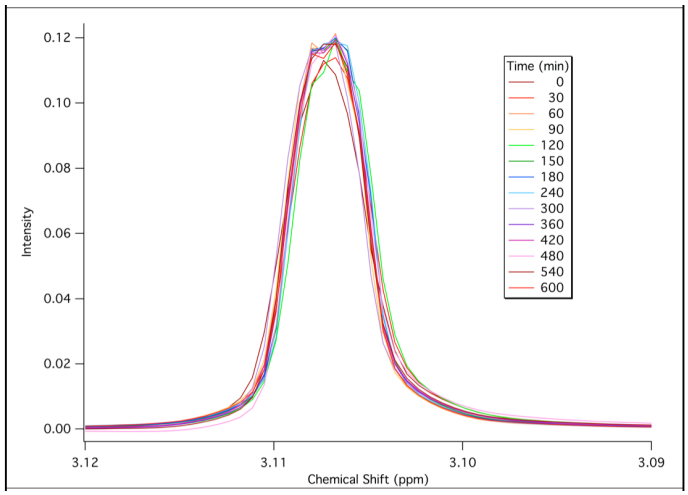


**Figure 20.** Normalization of the signal of the internal standard tetramethyl ammonium chloride at 3.11 ppm. Overlaid 1H NMR spectra of this signal shows normalization to constant intensity (concentration).

After normalization, overlaid spectra in Figure 21 show reactant peaks decreasing and product peaks growing in. This demonstrates that products did in fact form, and not that the terpineol concentration just decreased. The evaporation of α-terpineol was observed but at rates 2.5, 5.1, and 9.5 times slower than its reactivity for low (131 ppb), mid (480 ppb), and high (965 ppb) ozone concentrations, respectively. This is especially evident in Figure 22 in which the terpineol signal at 5.41 ppm decreases to almost zero intensity, and product signals at 5.29 and 5.34 ppm grown in from zero intensity.

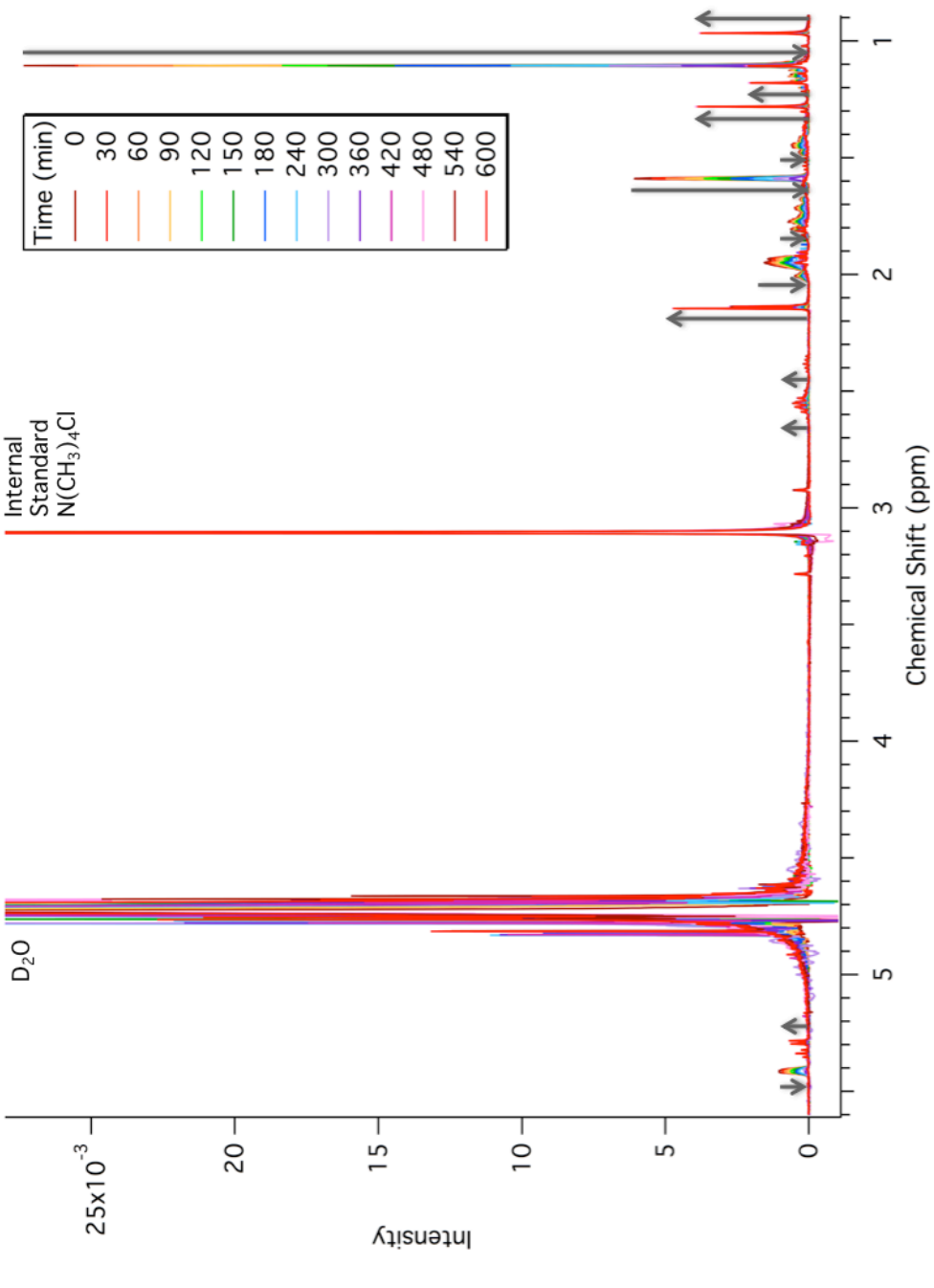


**Figure 21.** Overlaid $^{1}$H NMR spectra at time points 0-600 min. demonstrate reaction progress. Terpineol signals such as 1.1 ppm decrease to zero intensity. Product signals such as 2.15 ppm grow in from zero intensity.

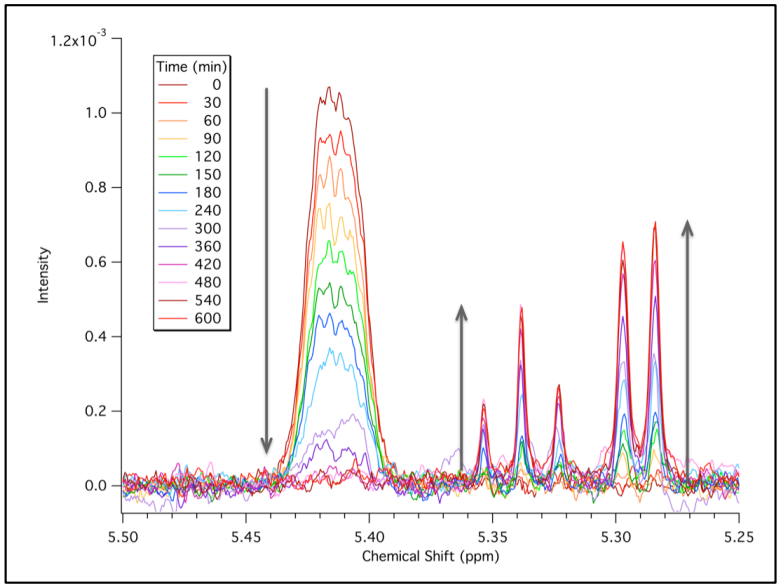


**Figure 22.** Overlaid 1H NMR spectra of chemical shift range 5.25-5.50 ppm at time points 0-600 min. Decreasing of terpineol signal (5.41 ppm) demonstrates using up of terpineol. Growing in of product signals (5.29 and 5.34 ppm) demonstrates formation of products distinct from terpineol.

### *3.2 Product Identification*

***3.2.1 Minor Product: Lactone*** Upon gas chromatography/mass spectrometry (GCMS) analysis of the product mixture in chloroform, four products eluted at retention times (RT) 12.75, 17.16, 20.03, and 22.22 min., as shown in Figure 23. The largest peak was found at RT 20.03 min. meaning it corresponds to the major product(s). The mass spectra were compared with mass spectra in the NIST Library resulting in the following matches—(*E*)-1,1-dimethyl-2-(2-methylhex-3-en-2-yl)cyclopropane as RT 12.75 min. (10.4% reliability); 5-(2-hydroxypropan-2-yl)-2-methylcyclohex-2-en-1-one as RT 17.16 min. (39.2% reliability); 5-(2-hydroxypropan-2-yl)-2-methylcyclohex-2-ene-1,4-diol as RT 20.03 min. (28.7% reliability); and 5,5-dimethyl-4-(3-oxobutyl)dihydrofuran-2(3H)-one as RT 22.22 min (96.3% reliability). Only the minor product RT 22.22 min. had significant reliability for its identification as 5,5-dimethyl-4-(3-oxobutyl)dihydrofuran-2(3H)-one, hereafter referred to as lactone (Figure 24).

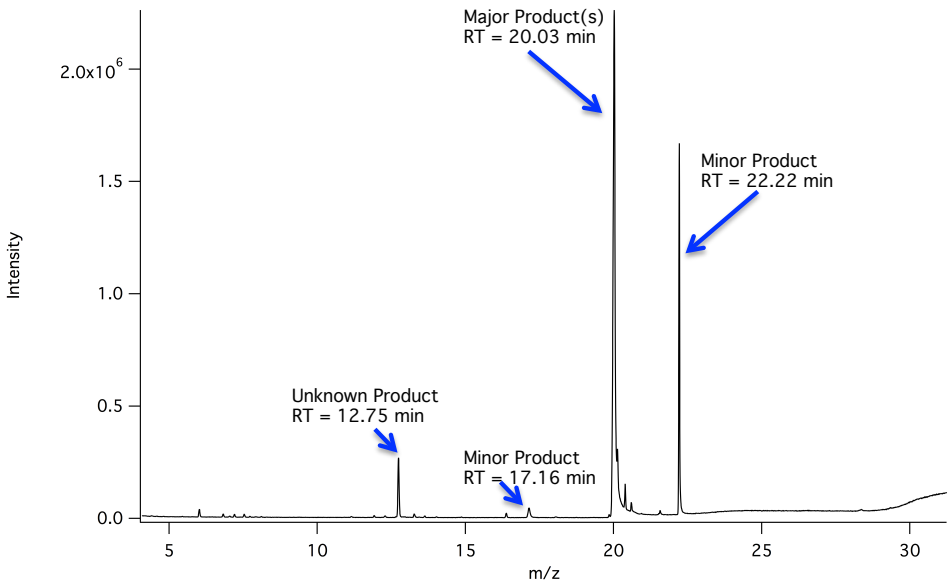


**Figure 23.** Gas chromatogram of aqueous product mixture in chloroform solvent showing four to five products present.

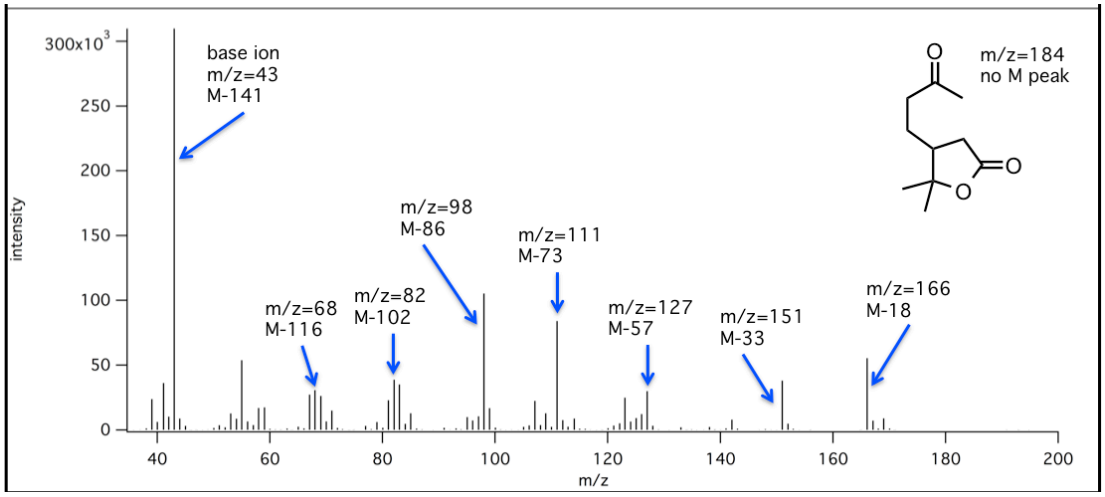


**Figure 24.** Mass spectrum of peak with retention time of 22.22 min. Comparison of mass spectrum with NIST library identified the product as lactone with 96.3% reliability.

To confirm the identification of the lactone, a derivatization technique was utilized in which BSTFA/10%TMCS reagent was added to the product mixture. The BSTFA reagent replaces the H of any alcohol group with a trimethylsilane (TriMS) group. TriMS groups are very polarizable which increases the ionization intensity in the GCMS. When BSTFA/10%TMCS reagent was added, the RT of the lactone did not change (Figure 25) and the mass spectrum did not change (Figure 26), therefore the lactone peak did not derivatize. Since this peak did not derivatize, the structure cannot have any alcohol groups on it, which agrees with the proposed lactone structure.

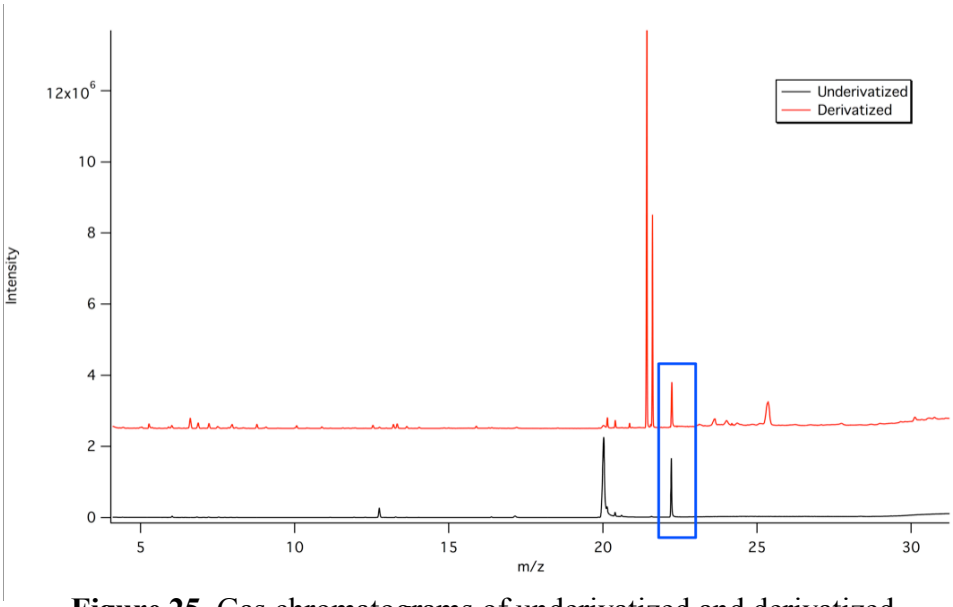


**Figure 25.** Gas chromatograms of underivatized and derivatized aqueous product mixture in chloroform solvent. The blue box indicates the unchanged lactone peak (RT 22.2 min) upon derivatization.

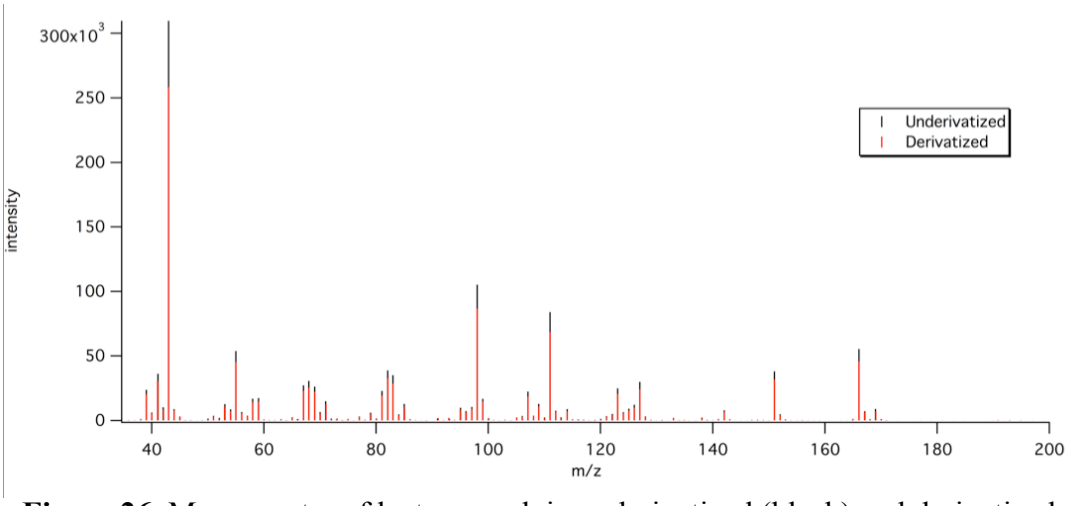


**Figure 26.** Mass spectra of lactone peak in underivatized (black) and derivatized (red) product mixtures. Mass fragmentation patterns are identical demonstrating that lactone did not derivatized and does not contain any alcohol groups.

Comparison of the product mixture with purchased lactone standard showed similar mass fragmentation patterns (Figure 27). This confirmed identification of the lactone as the minor product at 22.22 min. Further confirmation was successful by comparing the product mixture with $^{1}$H NMR and Infrared Spectroscopy (IR).

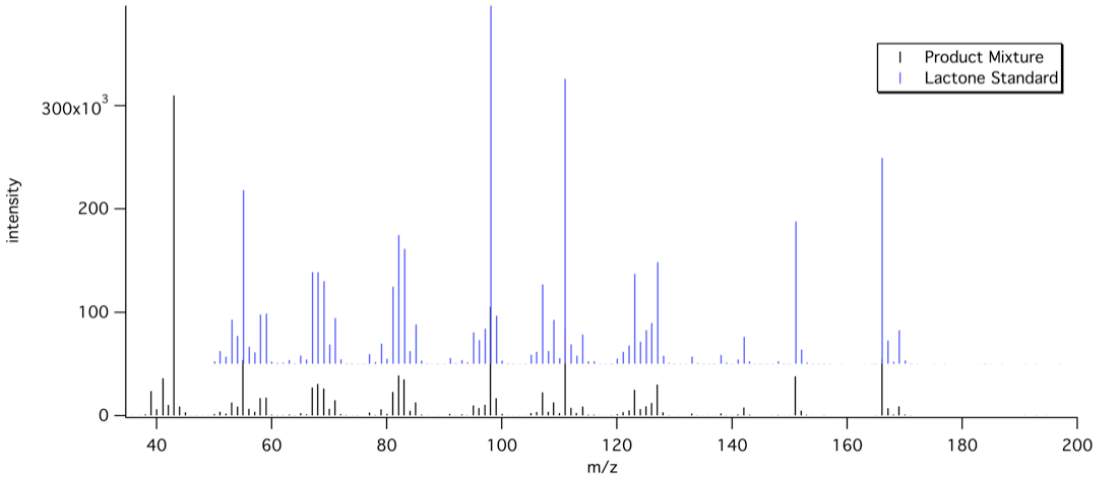


**Figure 27.** Mass spectra of lactone peak in product mixture (black) and in lactone standard (blue). Mass fragmentation patterns are very similar demonstrating that the lactone is the structure for the peak with retention time 22.22 min.

Comparison of the product mixture with the lactone standard in Figure 28 show that each of the $^{1}H$ signals of the lactone standard match to a signal in the product mixture. This demonstrates that the product mixture likely contains the lactone. Comparison of the IR spectra of the product mixture and the lactone standard in Figure 29 shows that each absorption of the lactone standard match to an absorption in the product mixture. For example, a key feature in the lactone standard is the carbonyl absorption at approximately 1700 $cm^{-1}$, which is also present in the product mixture. A key feature in the product mixture, but not found in the lactone is the alcohol absorption over the range of 3100-3500 $cm^{-1}$, showing that lactone does not contain any alcohol groups. This agrees with the GCMS derivatization results.

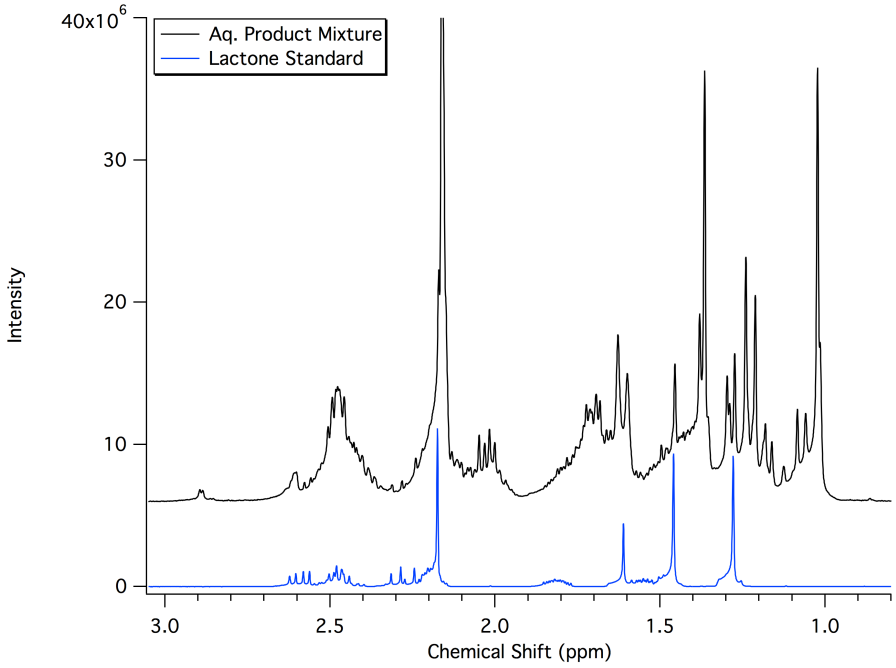


**Figure 28.** $^{1}H$ NMR spectra of the aqueous product mixture extracted into deuterated chloroform and lactone standard in deuterated chloroform, over the full chemical shift range of lactone (1-3 ppm). Each lactone standard signal matches to a signal in the aqueous product mixture demonstrating that the lactone is likely in the product mixture.

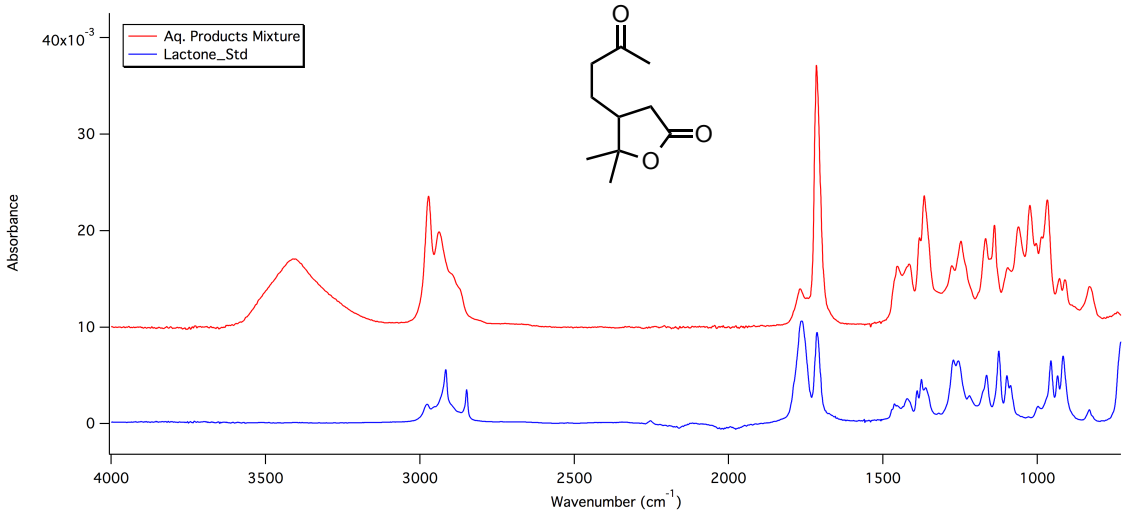


**Figure 29.** Infrared spectra of the aqueous product mixture extracted into deuterated chloroform and lactone standard in chloroform, over wavenumber range of 760-4000 $cm^{-1}$. Each lactone standard peak matches to a peak in the aqueous product mixture demonstrating that the lactone is likely in the product mixture. Both spectra have a carbonyl peak (1700 $cm^{-1}$) which agrees with the structure of lactone. The lactone spectrum lacks an alcohol peak (3100-3500 $cm^{-1}$) which agrees with its structure.

The ozonolysis of terpineol was conducted in reaction environments other than aqueous. These included a thin film of terpineol on glass, adsorbed on NaCl (for 2 and 5 hours) to model sea salt aerosols, and adsorbed on kaolinite to model mineral dust. The resulting product yield ratios, according to GCMS, are shown in Figure 30. The same four products result in each reaction environment; however, their ratios clearly differ among the reaction environments. For example, the lactone is a minor product in the aqueous environment (13.08%), but a major product on kaolinite (55.20%).

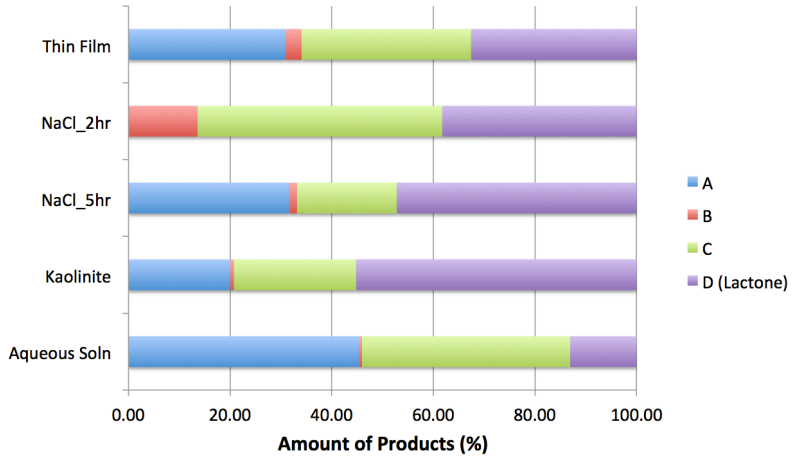


**Figure 30.** Product yield ratios according to GCMS for four compounds in the product mixtures. Ratios differ among reaction environments. Lactone is a minor product in aqueous environment (13.08%), but major product on kaolinite (55.20%).

The GCMS and IR data of the different reaction environments were compared. The ratios of C=O absorption to C-H absorption from the IR were compared to the lactone yield percentage from the GCMS (Figure 31). The figure demonstrates a direct linear relationship between the absorption ratios and the lactone yield. The trend appears to have a non-zero y-intercept suggesting that at least one product besides the lactone must have one carbonyl.

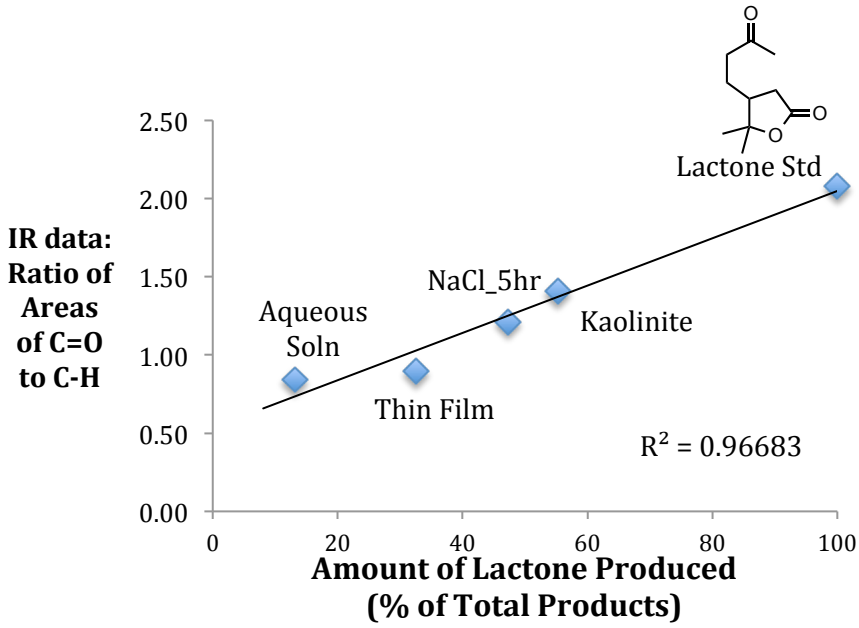


**Figure 31.** Comparison of the ratio of carbonyl to carbon-hydrogen (IR) to the lactone yield (GCMS) demonstrate that at least one product besides the lactone must have at least one carbonyl.

The proposed mechanism (Scheme 6) for the formation of lactone is consistent with the literature.[50] The initial reaction steps follow typical ozonolysis in which terpineol and ozone form the primary ozonide (POZ), then rearrangement forms the Criegee intermediate (CI), followed by addition and removal of water to form the lactone.

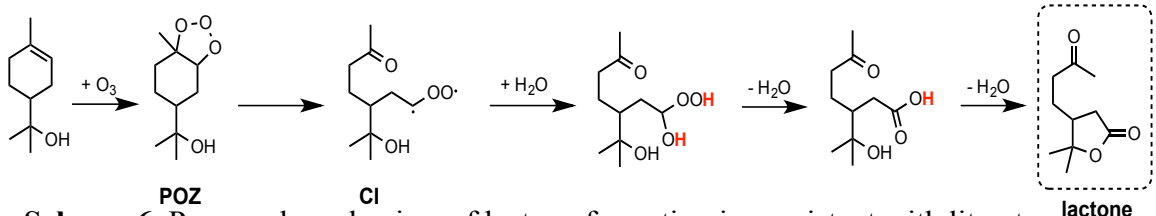


**Scheme 6.** Proposed mechanism of lactone formation is consistent with literature. Terpineol and ozone react to form the POZ. Further rearrangement forms the CI. After addition and removals of water, the lactone is formed.

In our experiment, we used deuterated water, so we would expect the hydrogen atoms ($^1$H) added by water to be deuterium atoms ($^2$H) instead. These are labeled red in Scheme 6. However the loss of water in the mechanism to form the lactone means that deuterium atoms are not expected in the lactone in our product mixture.

***3.2.2 Major Products: Key Features*** One of the most analyzed features in this research is the triplet and doublet $^1$H NMR peaks at 5.34 and 5.29 ppm, respectively (Figure 32b), and collectively referred to as the 5.3 ppm peaks. These signals fall in the 4.5-7.7 ppm chemical shift range of alkenes.[45] However, as ozone is very reactive with alkenes it is unlikely for a C=C bond to remain stable in the presence of ozone.[51] Another possibility for these chemical shifts is a methine proton alpha to two O atoms and one C atom. A method for roughly estimating chemical shifts is Shoolery's rule:

$$\delta = 0.23 + \Delta_X + \Delta_Y + \Delta_Z,$$

where $\delta$ is the chemical shift of the proton of interest; 0.23 ppm is the base chemical shift of methane; and $\Delta_X$, $\Delta_Y$, and $\Delta_Z$ are substituent parameters.[45] According to Shoolery's rule, each alpha oxygen substituent adds 2.36 ppm and the alpha carbon adds 0.47 ppm, yielding an estimated value of 5.42 ppm for this type of proton. Another estimation method uses the Curphey-Morrison parameters in which additivity constants of substituents alpha and beta to the proton's carbon are added to the base shift for the type of proton of interest (methane, methylene, or methine).[52] With this method, the base shift for a tertiary CH is 1.55 ppm to which 2.10 ppm is added for each alpha oxygen, yielding an estimated value of 5.75 ppm. The observed chemical shifts of 5.34 and 5.29 ppm are both within in 0.5 ppm of the estimated values, making either type of proton a possibility for the observed data.

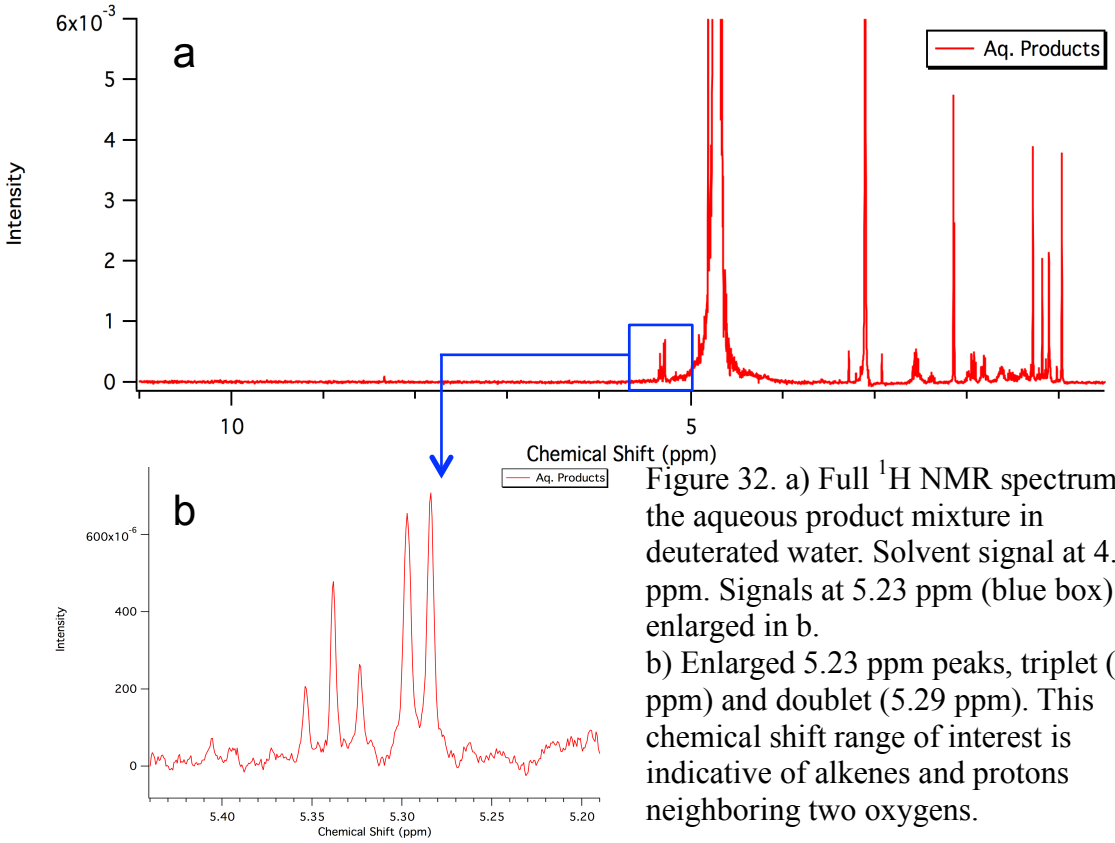


Figure 32. a) Full $^1$H NMR spectrum of the aqueous product mixture in deuterated water. Solvent signal at 4.7 ppm. Signals at 5.23 ppm (blue box) enlarged in b.
b) Enlarged 5.23 ppm peaks, triplet (5.34 ppm) and doublet (5.29 ppm). This chemical shift range of interest is indicative of alkenes and protons neighboring two oxygens.

Infrared spectroscopy confirmed the absence of alkenes in all of the products. The full IR spectrum is shown in Figure 33. The blue box indicates the alkene (C=C) region of 1610-1680 $cm^{-1}$, in which no absorptions are present. The green box indicates the carbonyl (C=O) region of 1690-1760 $cm^{-1}$, in which a strong absorption is present. The orange box indicates the aldehyde (C-H) region of 2700-2900 $cm^{-1}$, in which no characteristic aldehyde absorptions are present. In an IR spectrum, aldehyde absorptions are weak and appear as a doublet, and there is no doublet observed in the 2700-2900 $cm^{-1}$ region.[53] Also, when an aldehyde is present, one might see a wider C=O band, but the observed C=O band is sharp and has a small half-width. Aldehydic protons are very deshielded with high chemical shifts in the range of 9.70-10.3 ppm. The full $^{1}H$ NMR spectrum in Figure 32a shows an absence of signals in that region, concluding none of the products contain an aldehyde.

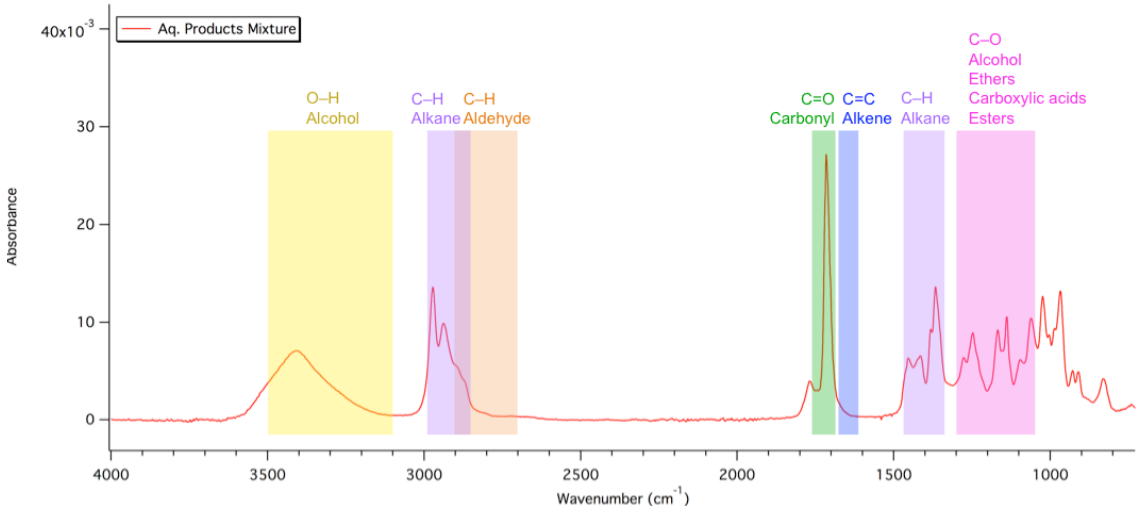


**Figure 33.** Infrared absorbance spectrum of aqueous products mixture. Yellow represents alcohol region (3100-3500 $cm^{-1}$). Purple represents alkane region (2850-2970 $cm^{-1}$, 1340-1470 $cm^{-1}$). Orange represents aldehyde region (2700-2900 $cm^{-1}$). Green represents carbonyl region (1690-1760 $cm^{-1}$). Blue represents alkene region (1610-1680 $cm^{-1}$). Pink represents carbon-oxygen single bond region (1050-1300 $cm^{-1}$).

The yellow box in Figure 33 indicates the alcohol region of 3100-3500 $cm^{-1}$, in which a broad absorption is present. The pink box indicates the carbon-oxygen bonds (C-O) of alcohols, ethers, carboxylic acids, and/or esters region of 1050-1300 $cm^{-1}$, in which absorptions are present. The purple boxes indicate the alkane regions (C-H) of 2850-2970 $cm^{-1}$ and 1340-1470 $cm^{-1}$, in which absorptions are present. Since the IR data eliminates the possibility of the 5.3 ppm peaks being alkenes, it is more likely they represent methine proton(s) alpha to two oxygens and one carbon atom.

An initial hypothesized structure including this feature is the secondary ozonide (SOZ). The SOZ is a known intermediate of ozonolysis, but is usually thought to be unstable and rarely isolated. However, some researchers claim that under aqueous conditions the SOZ can be isolated.[35, 38, 40] Some studies of aqueous ozonolysis of monoterpenes have shown that the Criegee intermediate stabilizes after forming from the decomposition of primary ozonide (POZ), which cannot be done in the gas phase.[35, 54] Recent studies have discussed the presence of water during ozonolysis of terpenes as a reason for the stability of a secondary ozonide formed as a product.[38] In ChemBioDraw, the $^{1}H$ NMR of the SOZ of α-terpineol shown in Figure 34 was predicted to have a peak at 5.30 ppm, which is consistent with the observed data and the Shoolery and Curphey-Morrison estimations. The predicted signal has a triplet pattern due to two neighboring protons, which matches the observed $^{1}H$ NMR spectrum. Therefore, the 5.30 ppm peaks initially presumed to be vinylic, could be indicative of the SOZ. The theoretical ChemBioDraw NMR suggests the triplet correlated to two neighboring protons of 1.5 ppm.

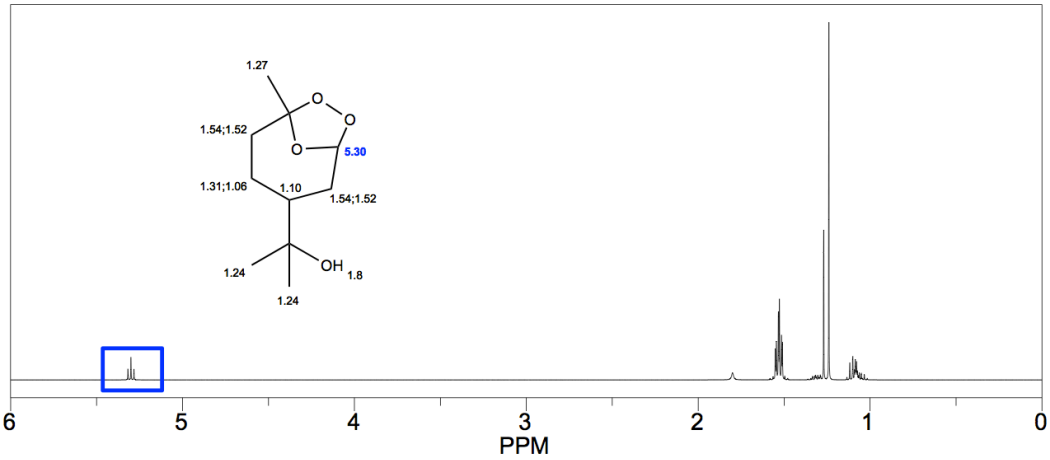


**Figure 34.** ChemNMR estimation of SOZ $^{1}$H NMR predicts a triplet signal at 5.30 ppm (blue).

Another key feature of the product mixture is that upon derivatization with BSTFA, the largest major GCMS peak (RT 20.03 min) presumably splits into two distinct, yet similar peaks (RT 21.4 and 21.6 min), shown in Figure 35. The mass spectra (Figure 36) of the two derivatized major peaks have nearly identical mass fragmentation patterns, only differing by intensities. The mass fragmentation intensities of the 21.4 min peak are greater than that of the 21.6 min peak. The very similar retention times and nearly identical mass spectra suggest the structures of two major products are similar and are possibly isomers.

Derivatization with BSTFA produced characteristic mass fragmentation patterns. BSTFA replaces the hydrogen atom of alcohol groups with a TriMS group. In MS, the ion m/z = 73 and M-73 are observed when one TriMS group is added. This is observed and shown in Figure 36. If additional TriMS groups are added, for example two TriMS groups, the ion m/z 147 and M-147 would be expected. This is not observed. Only the ion m/z = 73 and M-73 are observed. This indicates there is only one alcohol group on each of the similar structures.

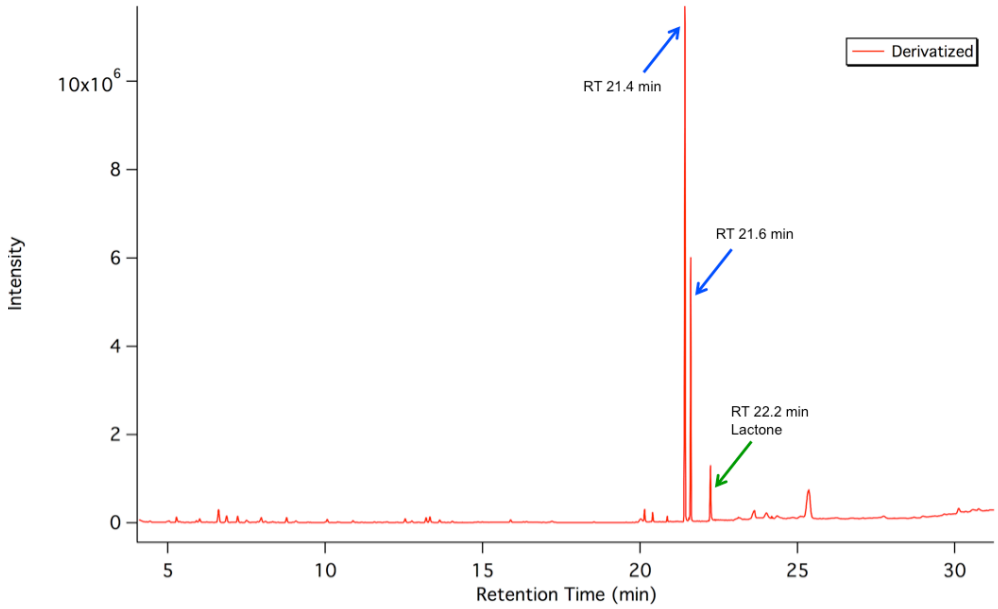


**Figure 35.** Gas chromatogram of derivatized aqueous product mixture in chloroform solvent. The blue arrows indicate the two major peaks with similar retention times 21.4 and 21.6 min upon derivatization. The green arrow indicates the lactone peak (RT 22.2 min).

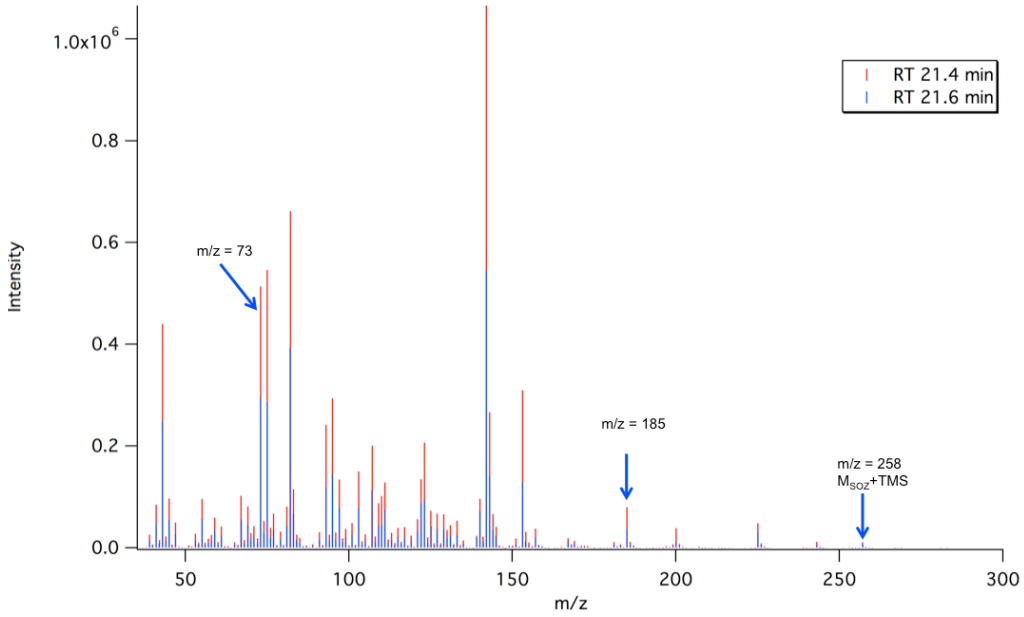


**Figure 36.** The mass spectra of RT 21.4 and 21.6 min of the derivatized sample have nearly identical mass fragmentation patterns. The fragment m/z = 73 is associated with the loss of the TMS group. The fragment m/z = 185 is observed. The fragment m/z = 258 is observed and could be the theoretical molecular ion of the SOZ with TMS group.

The proposed SOZ of α-terpineol is expected to maintain the alcohol group of its starting material. The SOZ structure is consistent with the derivation evidence of one alcohol group. Known fragments of SOZ are M-17 (m/z = 185) and M-34 (m/z = 168) assigned as losses of OH and $H_2O_2$, respectively, are observed.[31] However, in the underivatized mass spectrum of RT 20.03 min, the SOZ molecular ion (m/z = 202) is not observed. Also, M-1 (m/z = 201), a known fragment for alcohols corresponding to the loss of hydrogen is not observed.[55] In the derivatized mass spectrum of RT 21.4 and 21.6 min, the theoretical molecular ion of the SOZ (m/z = 202+72 = 274) is not observed. The observed base peak M-159 (m/z = 43) can be structurally explained by the breaking of the ozonide ring and the retaining $OCCH_3$ as the fragment. However, this is a complicated fragmentation and unlikely to be the most stable ion. Also, the SOZ structure cannot explain major fragments such as m/z = 58, 71, 95, 110, 128, and 153. In conclusion, the SOZ must be rejected as a possible product because it is not consistent with the mass fragmentation, existence of two derivatized peaks, and doublet $^1$H NMR signal.

***3.2.3 Major Products: Lactol Isomers*** The two major peaks of the derivatized chromatogram have very close retention times (21.4 and 21.6 min) within 0.2 min of each other. Their mass spectra are nearly identical and likely isomers. However, in the underivatized chromatogram only one major peak is found with a retention time of 20.03 min. The difference between the derivatized and underivatized data suggests that in the derivatized sample, the added TMS groups make the isomers different enough from each other for the instrument to detect them as different molecules. It also suggests that in the

underivatized sample having the alcohol groups intact with a hydrogen atom makes the isomers too similar for the instrument to detect them as separate molecules. It is logical to conclude this because TriMS groups are much larger than the hydrogen atom they are replacing which means there is more steric strain with the TriMS group yielding isomers that are more significantly different.

In analyzing the fragmentation pattern of the major product, the proposed compound is an α-hydroxyfuran or lactol with the alcohol group on the alpha carbon, a butanone group on the gamma carbon, and two methyl groups on the delta carbon (Figure 37a). This structure has two chiral centers at the alpha and gamma carbons, which yields two diasteromers, cis-lactol and trans-lactol (Figure 37 b & c). The cis and trans denote the orientation of the chiral $C_{alpha}$-O bond relative to the chiral C-$C_{gamma}$ bond.

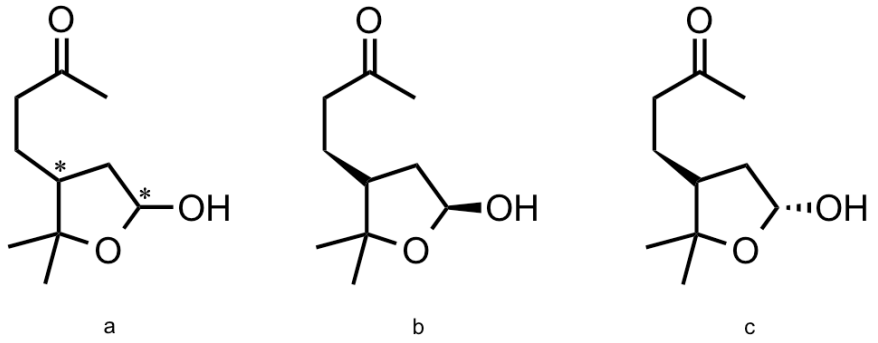


**Figure 37. a)** Proposed lactol major product with two chiral centers at the alpha and gamma carbons yielding two diasteromers **b** and **c**. **b)** cis-lactol **c)** trans-lactol
Note: Cis and trans denote the orientation of the chiral $C_{alpha}$-O bond relative to chiral C-$C_{gamma}$ bond.

The labeled mass spectrum of the underivatized major peak is shown in Figure 38. The mass spectra of the major and lactone peaks are similar, especially their base peaks (m/z = 43), a known fragment (-$COCH_3$) from the butanone side chain. The molecular

ion M peak (m/z = 186) is not observed, but the M-1 fragment (m/z = 185) is observed. The observed M-18 and M-33 fragments (m/z = 168 and 153, respectively) are consistent with the loss of water and the loss of both water and a methyl group, both known alcohol fragments.[55] The observed M-58 fragment (m/z = 128) is consistent with

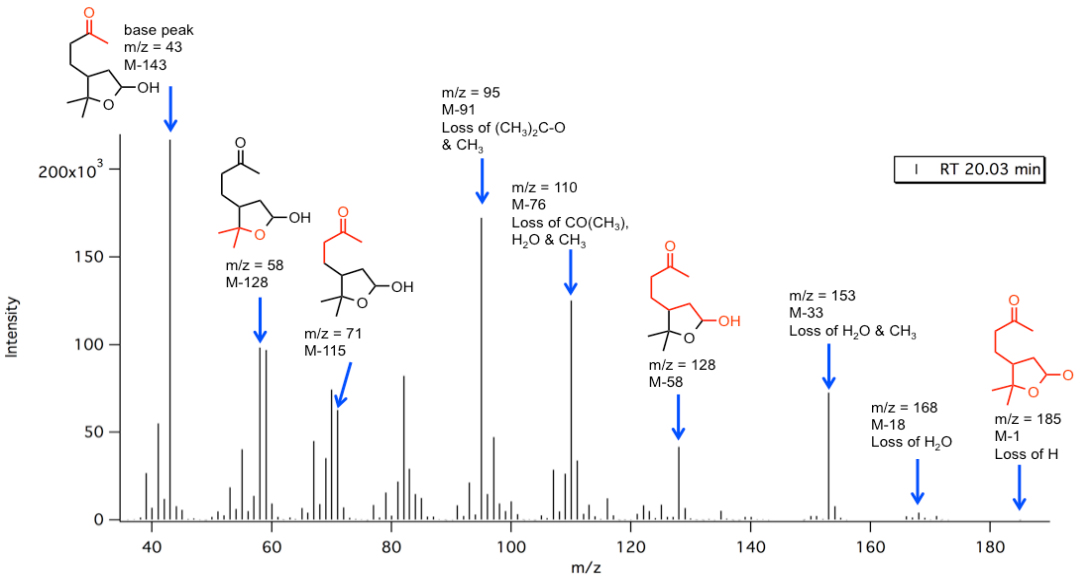


**Figure 38.** Labeled mass fragmentation pattern of underivatized 20.03 min peak. On structures, red indicates m/z fragment and black indicates lost fragment.

the loss of the furan/ring oxygen, delta carbon, and two methyl groups. The observed M-128 fragment (m/z = 58) is consistent with the loss of the M-58 fragment, which is the alpha, beta, and gamma carbons and the butanone side chain. The observed M-76 fragment (m/z = 110) is consistent with the loss of both the m/z = 43 (-$COCH_3$ from the butanone side chain) and m/z = 33 (water and methyl) fragments. The observed M-91 fragment (m/z = 95) is consistent with the loss of the m/z = 58 fragment and an additional methyl group. The M-115 fragment (m/z = 71) is consistent with the loss of a hydroxyfuran ring. Derivatization also produced the theoretical molecular ion (m/z = 186+72 = 258) as expected (Figure 36).

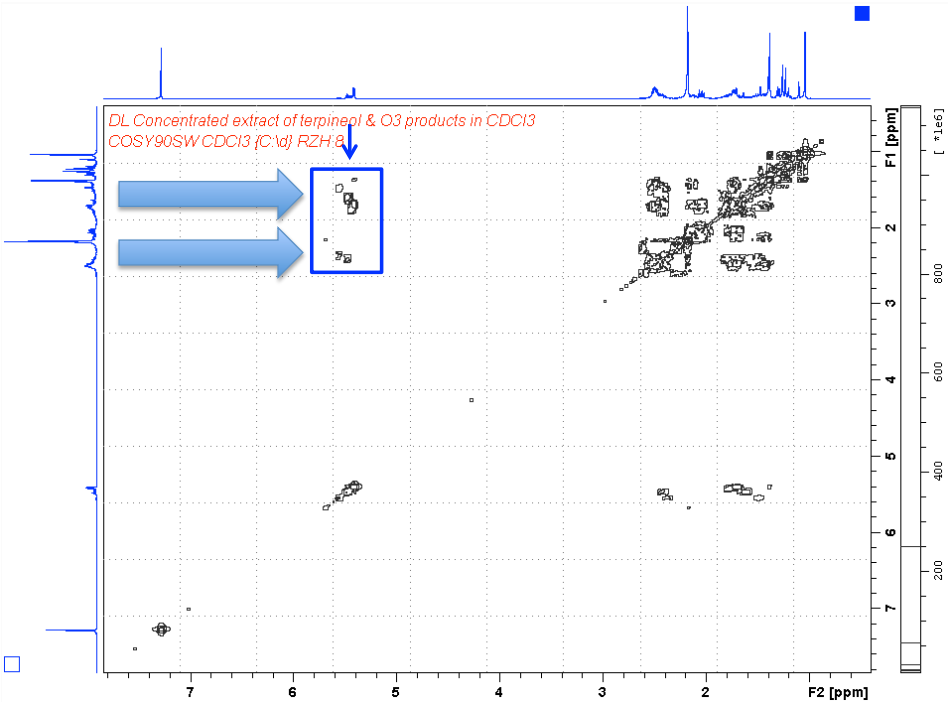


**Figure 39.** COSY spectrum of product mixture.

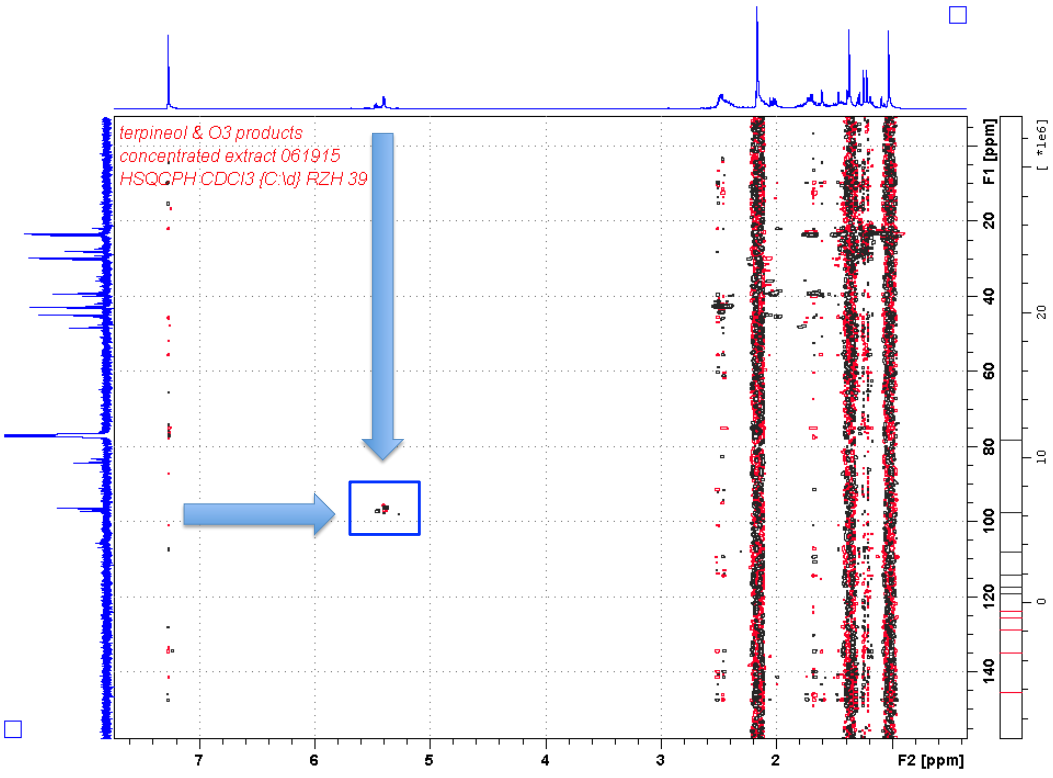


**Figure 40.** HSQC spectrum of product mixture.

This proposed lactol structure contains the proton of interest, a methine proton alpha to two oxygen atoms and a carbon atom, which is consistent with the observed $^{1}H$ NMR signals at approximately 5.30 ppm. The two-dimensional (2D) NMR spectra, COSY and HSQC, are shown in Figures 39 and 40, respectively. Due to the presence and similarity of multiple compounds in the product mixture, the two-dimensional NMR spectra are difficult to completely analyze all cross sections. However, they are consistent with the proton of interest. On the COSY spectrum of the products (Figure 39), the blue box indicates the cross-section of the proton of interest's triplet and doublet corresponding to neighbors in the 1.2-1.8 ppm and 2.2-2.5 ppm ranges, which is consistent with the proposed structure. On the HSQC spectrum of the products (Figure 40), the blue box indicates the cross-section of the triplet and doublet of the proton corresponding to the carbon at approximately 95 ppm, which is consistent with the proposed structure. ChemDraw predicts this carbon to be at 102 ppm.

However, the GCMS data does not explain why two different splitting patterns (triplet and doublet) are observed in the 5.30 ppm region. Structures of the cis and trans lactol were optimized in Gaussian in water solvent conditions. In both isomers, the proton of interest neighbors two protons. When viewing down the $C_{alpha}$-$C_{beta}$ bond of the optimized structures (Figure 41), the dihedral angles between the proton of interest (circled in blue) and its neighbors (blue arrows) are different for the two isomers. In the cis isomer, atom 6 (proton of interest) is almost 180˚ from atom 7 (neighbor) and less than 45˚ from atom 8 (neighbor). In the trans isomer, atom 29 (proton of interest) is less than 45˚ from atom 6 (neighbor) and about 90˚ from atom 7 (neighbor). According to the

Karplus equation, the cis isomer would have a non-zero coupling constant for atoms 6 and 7, and atoms 6 and 8, and the trans isomer would have a non-zero coupling constant for atoms 29 and 6 and an approximately zero coupling constant for atoms 29 and 7.

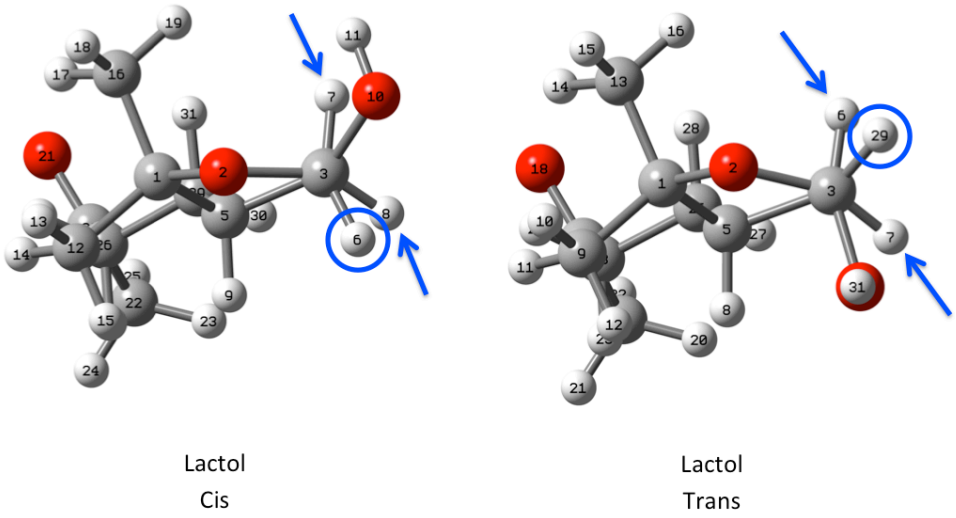


**Figure 41.** Optimized structures of lactol isomers (cis and trans) in Gaussian. Atoms circled in blue are the proton of interest which is on the same carbon as the alcohol group. Blue arrows point to their neighboring protons. The dihedral angles differ within and between each isomer.

**Table 5.** Theoretical coupling constants (J) of proton on alpha carbon. Note: "a" denotes proton of interest and "b" denotes neighboring proton.

| isomer | $H_a$ | $H_b$ | J Coupling (Hz) |
|---|---|---|---|
| cis | 6 | 7 | 7.38879 |
| cis | 6 | 8 | 6.32044 |
| trans | 29 | 6 | 5.71865 |
| trans | 29 | 7 | -0.0184957 |

The theoretical coupling constants are reported in Table 5. The cis coupling constants are similar and both non-zero for atoms 6 and 7 and atoms 6 and 8 (7.38879 and 6.32044 Hz, respectively), which is consistent with the Karplus equation. The trans coupling constants

is non-zero for atoms 29 and 6 (5.71865 Hz) and approximately zero for atoms 29 and 7 (-0.0184957 Hz), which is consistent with the Karplus equation. More research is needed to understand the reasoning for a negative coupling constant value.

The theoretical $^{1}$H NMR signal generated as Lorentzian functions are shown in Figure 42a compared to the experimental signals with the theoretical centers of the signals set to be the same as the experimental centers of the signals. The theoretical peak widths were arbitrarily selected for comparison with the experimental signals. The red function is the theoretical triplet (cis). The blue function is the theoretical doublet (trans). The green graph is the experimental. The signals overlap closely indicating the proposed lactol isomer structures have coupling constants consistent with the observed NMR data. However, when the theoretical chemical shifts of the signals are set to be the values computed by Gaussian, the result is less conclusive (Figure 42b). The theoretical and experimental chemical shifts are reported in Table 6.

**Table 6.** Theoretical and experimental $^{1}$H NMR centers (ppm) of proton of interest.

| Splitting Pattern | Theoretical Center (ppm) | Experimental Center (ppm) |
|---|---|---|
| triplet | 5.2488 | 5.3380 |
| doublet | 5.3442 | 5.2905 |

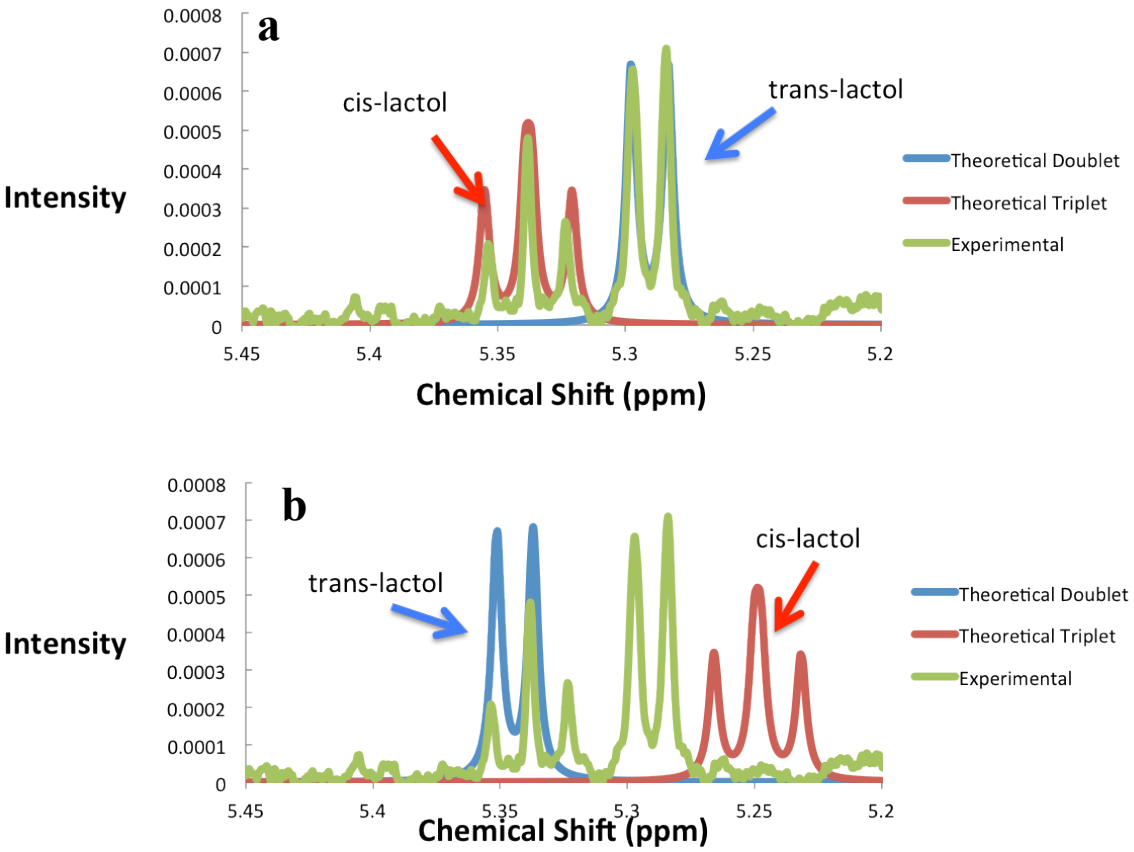


**Figure 42**. Comparison of theoretical and experimental $^{1}$H NMR for 5.30 ppm peaks (triplet and doublet). Peak widths are set arbitrarily. **a)** Theoretical chemical shift centers are set to be the same as the experimental centers, demonstrating that proposed lactol isomers consistent with experimental data at characteristic chemical shift region. **b)** Theoretical chemical shift centers are set as values computed by Gaussian. Theoretical centers do not match experimental centers.

The experimental results show the triplet at a higher chemical shift (more deshielded) than the doublet (5.3380 and 5.2905 ppm, respectively). The theoretical results report the triplet at lower chemical shift (more shielded) than the doublet (5.2488 and 5.3442 ppm, respectively). A possible explanation for the discrepancy between theoretical and experimental chemical shifts is a limitation of Gaussian in that the coupling constant

values computed are equivalent to a snapshot of the averaging that occurs in the actual NMR instrument.

The proposed mechanism (Scheme 7) includes the formation of lactone and lactol isomers and is consistent with literature.[50] According to the mechanism, in the formation of the lactol isomers, hydrogen peroxide is generated in the formation of the aldehyde precursor to the lactol isomers. Hydrogen peroxide is a known byproduct of ozonolysis in the presence of water.[56]

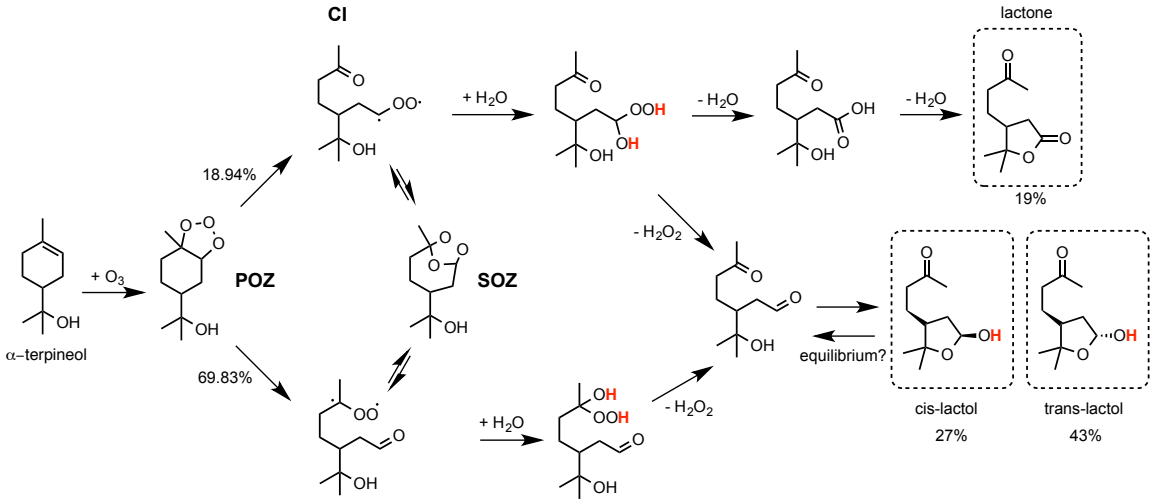


**Scheme 7.** Proposed mechanism consistent with literature and formation of $H_2O_2$.

Peroxide test strips tested positive during the course of the reaction for the presence of peroxide in the solution as shown by the blue color in Figure 43. The peroxide concentration approximated by the intensity of the blue color was plotted against reaction time (Figure 44) and shows peroxide concentration increases over time, indicating a buildup of peroxide as lactol isomer products form, which verifies the proposed mechanism.

**Figure 43.** Blue color of hydrogen peroxide test strip demonstrates presences of hydrogen peroxide in reaction solution.

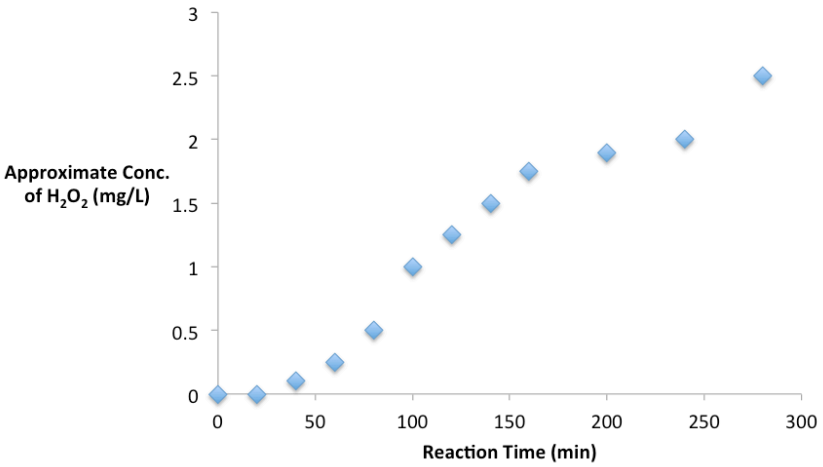


**Figure 44.** The semi-quantitative kinetic study of $H_2O_2$ formation during ozonolysis of terpineol demonstrates an increase in peroxide concentration during the course of the reaction.

In our experiment, we used deuterated water, so we would expect the hydrogen atoms ($^1$H) added by water to be deuterium atoms ($^2$H) instead. These are labeled red in Scheme 7. We would expect the alcohol group on the lactol to be deuterated if it originated from water. However, this is not observed in the underivatized mass spectrum because we only see the M-H peak (m/z = 185) which would be the same mass whether $^1$H (186-1=185) or $^2$H (187-2=185) is lost. The molecular ion for lactol (m/z = 186) and deuterated lactol (m/z = 187) are not observed. In addition, the presence of $^2$H is not observed in the derivatized mass spectra because derivation replaces the hydrogen or deuterated hydrogen of an alcohol with a TriMS group.

***3.3 Aqueous Phase Kinetics*** The variation of ozone concentration demonstrated that product formation of both lactol isomers is linearly dependent on ozone (Figure 45). This suggests that the reaction is first order with respect to ozone. The linear shape of each

curve suggests the reaction is zero order with respect to α-terpineol. This is unexpected, but may be due to the reaction occurring in a combination of in solution near the surface, in the bulk of the solution, or at the interface. A simple mechanism describing this observation,

$$O_3(g) \xrightarrow{slow} O_3(aq)$$

$$O_3(aq) + \text{terpineol}(aq) \xrightarrow{fast} \text{products}$$

$$\therefore \text{Rate} \approx k[O_{3(g)}]$$

in which the fast gas transport to the surface is followed by the slow step of ozone dissolving, followed by the fast reaction between ozone and α-terpineol.

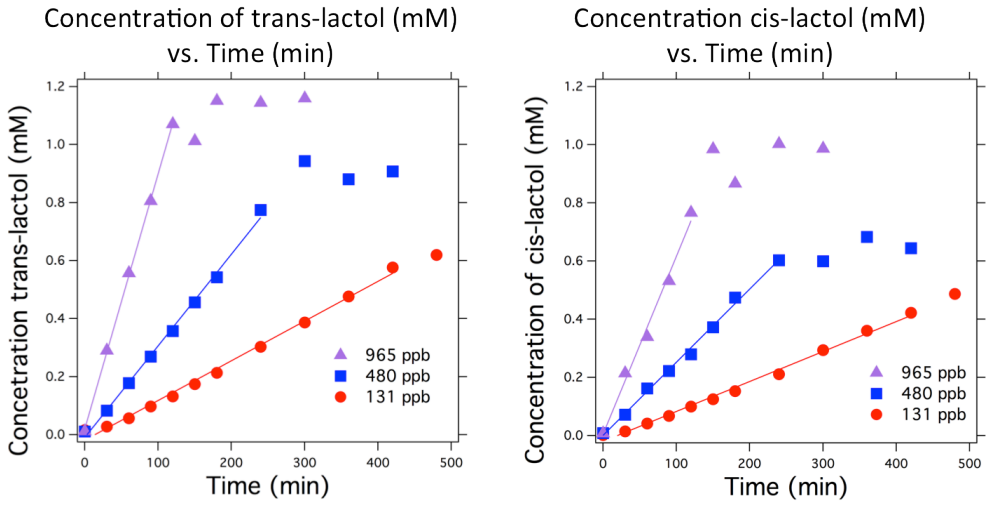


**Figure 45.** Rate of production formation is linearly dependent on ozone concentration. Trans-lactol and cis-lactol refer to the products with the doublet and triplet in the $^1$H NMR, respectively.

Ozone is hydrophobic as it has a low Henry's law coefficient, 1.00 x $10^{-2}$ M $atm^{-1}$. These ideas support the first step being slow. For the reaction to occur in solution, several steps must occur.[57] 1) Gaseous ozone diffuses to the droplet's surface where a

heterogeneous reaction may occur between gaseous ozone and dissolved α-terpineol. 2) In a process called uptake, ozone is transported across the air-water interface where the reaction can occur between dissolved ozone and dissolved α-terpineol. 3) The dissolved ozone diffuses into the droplet's aqueous bulk phase, and the reaction takes place in solution near the surface or in the bulk. However, diffusion of molecules in the aqueous phase is slower than in the gas phase. To determine the aqueous reaction's rate constant ($k$) and lifetime ($\tau$), and to ultimately compare aqueous ozonolysis of α-terpineol to that of gaseous ozonolysis, several values must be calculated.

For gaseous molecules of ozone to diffuse to the surface and into the droplet and ultimately react in solution, they must collide with the surface, but not all collisions with the surface will result in a reaction occurring. Reactive uptake coefficients ($\gamma$) describe the heterogeneous reaction kinetics as the fraction of $O_3$-water surface collisions resulting in a reaction,

$$\gamma = \frac{d[O_3]/dt}{Z}$$

where $Z$ is the frequency of $O_3$-water surface collision as determined by the kinetic theory of gases,

$$Z = \frac{A[O_3]}{4}\sqrt{\frac{8RT}{\pi M_{O_3}}}$$

where $A$ is the total surface area, $R$ is the gas constant, $T$ is the temperature, and $M_{O_3}$ is the molar mass of ozone.[58]

The net collisional uptake probability ($\gamma_{net}$) is the net rate of gaseous ozone uptake described in terms of conductances ($\Gamma$) normalized to the rate of $O_3$-water surface collisions,

$$\frac{1}{\gamma_{net}} = \frac{1}{\Gamma_g} + \frac{1}{\alpha} + \frac{1}{\Gamma_{rxn} + \Gamma_{sol}}$$

where $\Gamma_g$, $\Gamma_{sol}$, and $\Gamma_{rxn}$, are the conductances associated with gas-phase diffusion to the surface, solubility, and reaction in the bulk aqueous phase, respectively, and $\alpha$ is the mass accommodation coefficient across the interface.[57] The mass accommodation coefficient is the fraction of gas-condensed phase collisions resulting in uptake of gas. $\alpha_{O_3}$ has been found to have a lower limit of $2 \times 10^{-2}$, which is used in the present study.[59]

The previous equation has been shown to be equivalent to,

$$\frac{1}{\gamma_{net}} = \frac{1}{\Gamma_g} + \frac{1}{\alpha} + \frac{1}{\frac{4HRT}{u_{av}}\left[\sqrt{\frac{D_1}{\pi t}} + \sqrt{D_1 k}\right]}$$

which has several limiting cases for atmospheric reactions, and where $H$ is Henry's law coefficient for gas dissolving in condensed phase, $u_{av}$ is the mean thermal velocity of ozone in the gas phase, $D_1$ is the diffusivity of ozone in water, $t$ is time, $k$ is the pseudo first order rate constant, and remaining symbols are as defined earlier.[57] Mean thermal velocity is given by

$$u_{av} = \sqrt{\frac{3RT}{M_{O_3}}}$$

where variables are as defined earlier. The diffusivity of ozone in water is given by

$$D_1 = 1.10 \times 10^{-6} \exp\left[\frac{-1896}{T}\right]$$

where variables are as defined earlier.[60] The second order bulk aqueous rate coefficient is given by

$$k_{O_3}=k[\alpha\text{-terpineol}]$$

in units of $M^{-1}s^{-1}$. Henry's law coefficient for ozone in water has been found to be (0.82-1.3) x $10^{-2}$ M $atm^{-1}$, a low solubility, and in the present study the geometric mean, 1.0 x $10^{-2}$ M $atm^{-1}$, is used.[57] The earlier proposed reaction mechanism is a limiting case for the reactive uptake coefficient expressed by

$$\frac{1}{\gamma_{net}}=\frac{1}{\alpha}+\frac{u_{av}}{4HRT\sqrt{D_1 k}}$$

since $\Gamma sol << \Gamma rxn$.[57]

After determining the net reactive uptake coefficient and total surface collision frequency to calculate the reactive uptake (d[O3]/dt), the experimental data can be fitted kinetically by calculating the theoretical concentration of product for a given time (*t*)

$$[\text{Product}]=[\alpha\text{-terpineol}]_o+\frac{d[O_3]}{dt}(t-t_o)$$

where $[\alpha\text{-terpineol}]_o$ is the α-terpineol concentration at a preceding time ($t_o$).This fit and the rate constant (*k*) are optimized for each ozone concentration (131 ppb, 480 ppb, 965 ppb) separately by reducing the sum of the squared error of the theoretical and experimental product concentrations (Figure 46). The rate constants for each ozone concentration experiment are summarized in Table 7. The average rate constant for the aqueous ozonolysis of α-terpineol was found to be 9.93 x $10^6$ $M^{-1}s^{-1}$.

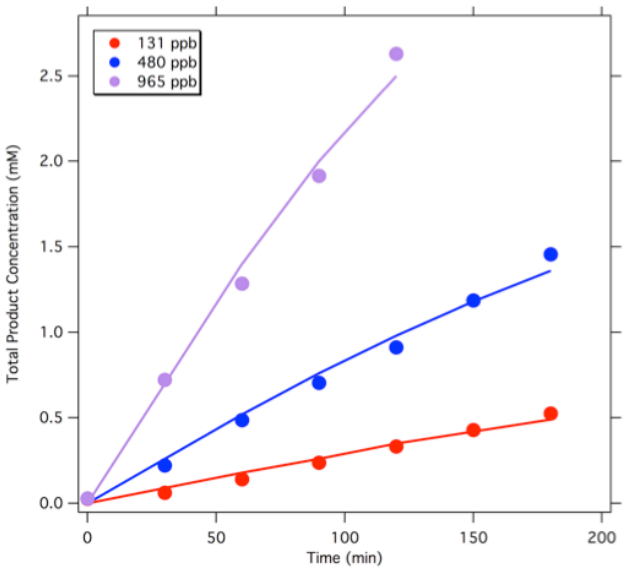


**Figure 46.** Kinetic fit of experimental data to theoretical rate constants.

**Table 7.** Rate constants for each ozone concentration experiment.

| **[Ozone] (ppb)** | **k ($M^{-1}s^{-1}$)** |
|---|---|
| 131 | $1.21 \times 10^{7}$ |
| 480 | $6.15 \times 10^{6}$ |
| 965 | $1.16 \times 10^{7}$ |

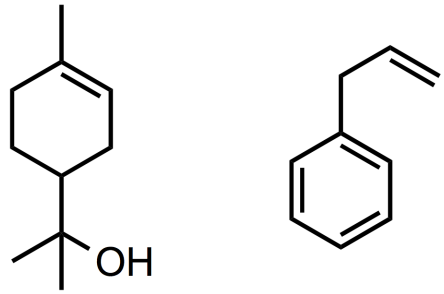


α-terpineol styrene

**Figure 47**. Structures of α-terpineol and styrene.

This is a relatively fast reaction as its rate constant is an order of magnitude faster than that of the aqueous ozonolysis of styrene ($k = 3.00 \times 10^5\ M^{-1}s^{-1}$), a structurally similar molecule (Figure 47).[61] This faster rate is likely due to the alkene attacked by ozone being more substituted on α-terpineol than it is on styrene.[62] Since these substituents are electron donating alkyl groups, the alkene has greater electron density. Ozone is an electrophile, which means it is attracted to electrons, so it will have a greater attraction to the alkene with greater electron density. This lowers the activation energy for the addition of ozone to the alkene of α-terpineol compared to that of the alkene of styrene.

The gas-phase ozonolysis of α-terpineol is described by the reaction

$$O_{3(g)} + \alpha\text{-terpineol}_{(g)} \longrightarrow \text{products}$$

$$\therefore \text{Rate} \approx k[O_{3(g)}][\alpha\text{-terpineol}_{(g)}]$$

with a reported rate constant, k, of $3.0 \times 10^{-16}\ cm^3\ molecules^{-1}\ s^{-1}$.[37] The gas and aqueous phases can be compared by comparing their lifetimes, $\tau$, which describe the length of time a reactant will exist in the atmosphere before reacting, and is the inverse of the overall rate constant of the reaction expressed by

$$\frac{1}{\tau} = k = k_{O_3}[O_3]$$

where $\tau$ is the lifetime, $k$ is the overall rate constant, $k_{O_3}$ is the rate constant with respect to ozone, and $[O_3]$ is the concentration of ozone in either the gas or aqueous phase. The reported 24 h daytime and nighttime average ozone concentration in the troposphere is used as the gaseous centration of ozone, $[O_{3(g)}] = 7 \times 10^{11}$ molecules $cm^{-3}$, which is

equivalent to 1.16 x $10^{-9}$ M.[63] For the gas-phase reaction, $\tau$ = 79 min. To calculate the aqueous phase concentration of ozone, $[O_{3(aq)}]$, $[O_{3(g)}]$ is converted to units of pressure (atm) using the Ideal Gas Law rearranged as,

$$P = \frac{n}{V}RT,$$

where *P* is pressure, *n/V* is $[O_{3(g)}]$, and remaining symbols are as defined earlier, which can then be used with Henry's law constant (1.14 x $10^{-2}$ M $atm^{-1}$)[63] to determine $[O_{3(aq)}]$, according to

$$[O_{3(aq)}] = PH,$$

which yields $[O_{3(aq)}]$ = 3.2 x $10^{-10}$ M. This concentration and the average aqueous ozonolysis rate constant ($k_{O3}$=9.93 x $10^6$ $M^{-1}s^{-1}$) yield a lifetime for the aqueous phase reaction, $\tau$ = 5.2 min. The lifetime of the aqueous reaction (a condensed phase) is 15 times faster than that of the gas-phase reaction, demonstrating the importance of the aqueous phase reaction.

The reported range for the second-order surface reaction rate constant ($k_2$) for the ozonolysis of α-terpineol adsorbed on glass, PVC, and vinyl is (0.68-3.17) x $10^{-16}$ $cm^4$ $molecules^{-1}$ $s^{-1}$. This is an unusual unit, but when the researchers multiplied this range of values to range of surface to volume ratios (*S/V*) in residences (0.029-0.046 $cm^{-1}$), the $k_2S/V$ range is (2-15) x $10^{-16}$ $cm^3$ $molecules^{-1}$ $s^{-1}$. This value was compared to the gas phase rate constant (3.0 x $10^{-16}$ $cm^3$ $molecules^{-1}$ $s^{-1}$), which prompted the conclusion that surface ozonolysis occurred at rates equal or higher than that of the gas-phase reaction, but with the same magnitude. It can be deduced that condensed phase ozonolysis occurs

faster than gas phase ozonolysis, which agrees with the aqueous phase reaction having a shorter lifetime than the gas phase reaction.

To compare the lifetimes of the surface and aqueous reactions, $k_2S/V$ and 24 h daytime and nighttime average ozone concentration in the troposphere are used to find the overall rate constant (k), the inverse of which is the lifetime ($\tau$). The range of lifetimes for the surface reaction is 15.9 to 119 min. The previously reported aqueous lifetime ($\tau$ = 5.2 min) demonstrates that the aqueous reaction is between 3 and 23 times faster than the surface reaction.

Further data reporting the concentration of ozone in solution must be collected. Kinetics data were collected using an open system, meaning that ozone could flow out and solvent could evaporate. A closed system experiment needs to be conducted in order to obtain more accurate kinetics data.

# Chapter 4. Conclusion

## *4.1 Implication of Products*

The ozonolysis of α-terpineol in an aqueous environment yielded two major product isomers of 4-((3*R*,5*S*)-5-hydroxy-2,2-dimethyltetrahydrofuran-3-yl)butan-2-one (trans: 42.61%, cis: 27.22%), one minor product 5,5-dimethyl-4-(3-oxobutyl)dihydrofuran-2(3*H*)-one (18.94%), and three unidentified minor products (4.65%, 1.55%, and 1.32%).

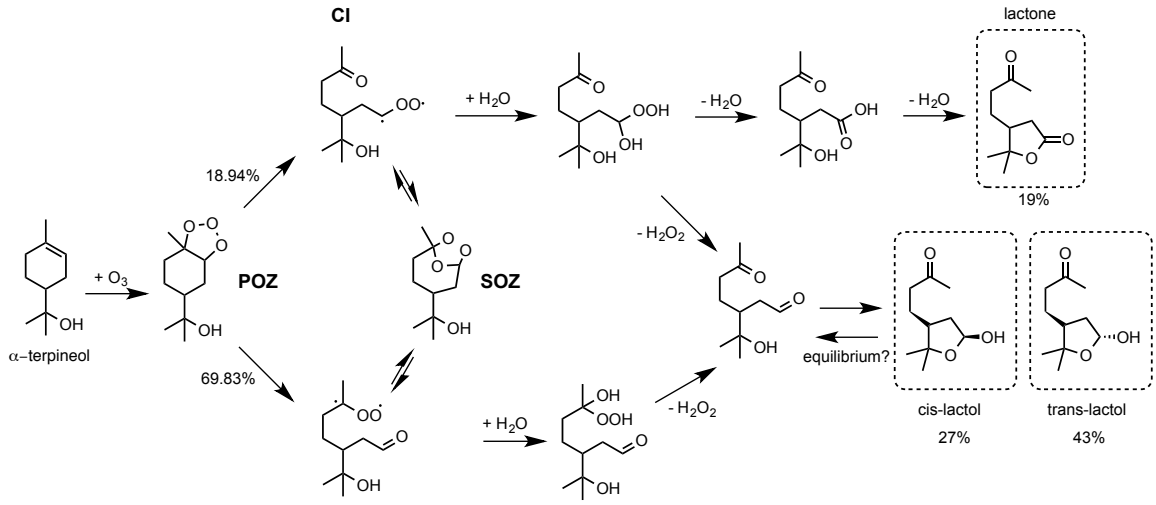


**Scheme 8.** Proposed mechanism of aqueous ozonolysis of α-terpineol consistent with literature and formation of $H_2O_2$.

The aqueous Henry's law constant of the lactol can be estimated using the two methods described by Brockbank, et al.[64] These methods are termed as a first order method and a second order method, not to be confused with first order and second order rate laws. The first order method parameterizes the contributions of groups. The second order method accounts for the interactions of neighbors of a group. Both methods have limitations with the first order not having a parameter for ether and the second order not having a parameter for alkenes which then must be treated as an aromatic C=C. The resultant

estimations for the Henry's law constants for α-terpineol and lactol using both methods are reported in Table 8. In both first and second order methods, lactol is 235 and 6.7 x $10^6$ times less volatile than α-terpineol, respectively.

**Table 8.** The theoretical Henry's law constants for α-terpineol and lactol.

| Compound | First Order Method (atm $M^{-1}$) | Second Order Method (atm $M^{-1}$) | Log Average (atm $M^{-1}$) |
|---|---|---|---|
| α-terpineol | 5.10 x $10^{-5}$ | 4.16 x $10^{-2}$ | 1.46 x $10^{-3}$ |
| lactol | 2.17 x $10^{-7}$ | 6.17 x $10^{-9}$ | 3.66 x $10^{-8}$ |

Comparing the log averages of the two methods used to estimate Henry's law constant for lactol (3.66 x $10^{-8}$ atm $M^{-1}$) to that of α-terpineol (1.46 x $10^{-3}$ atm $M^{-1}$), the lactol is 3.98 x $10^4$ less volatile than α-terpineol. All identified products are more oxidized than α-terpineol suggesting longer atmospheric lifetimes due to decreased volatility. The decreased volatility of these products enables them to exist in the condensed phase longer. These compounds may have greater solubility in water suggesting they may act as better cloud condensation nuclei, leading to the formation of denser clouds with higher albedo values which means these whiter clouds would reflect more light back into space, and leave less energy to heat the Earth's surface resulting in a global negative RF value (net cooling effect). This study also reports for the first time the rate constant for aqueous ozonolysis of α-terpineol (9.93 x $10^6$ $M^{-1}s^{-1}$), which is an order of magnitude faster than that of the gas phase reaction (1.8 x $10^5$ $M^{-1}s^{-1}$). This suggests that the aqueous phase reaction is more important than the gas phase reaction.

The results of this study are also relevant to indoor air quality. Air purifiers can produce ozone intentionally or as an air ionization byproduct, resulting in dangerous concentration levels without proper ventilation. According to the U.S. Environmental Protection Agency, levels of ozone above 120 ppb for 1-hr exposure and 80 ppb for 8-hr exposure present a risk of respiratory symptoms and reduced lung function.[65] Britigan et al. measured steady-state ozone concentrations during operation of nine air purifiers in various indoor environments such as bathrooms, bedrooms, offices, and cars. The measured ozone concentrations had a range of 9-650 ppb, with 72% of the measurements at or above the EPA risk levels.[66] These high concentrations of ozone alone have health implications. However, the reaction of ozone with organic aerosols such as α-terpineol, which are present in household cleaners and perfumes, can yield secondary organic aerosols like lactol, which have longer lifetimes. Shu et al. have studied ozonolysis of α-terpineol on common indoor surfaces, glass, PVC, and latex paint, finding reaction probabilities on surfaces to be larger than in the gas phase.[43] The aqueous environment, such as the phase studied in the present research, can exist in indoor air environments because of natural humidity and humidifiers, which renders the present study of relevance to indoor air environments.

The conclusive rejection of the secondary ozonide (SOZ) as a product and the subsequent identification of the major products as lactol isomers questions the observation of the SOZ by NMR in the study by Maksymiuk et al.[44] The $^{1}$H NMR signal these researchers attribute to the methine proton of SOZs, 5.6-5.8 ppm, is in a similar region to the proton of interest in the present study (5.3 ppm), which has been identified

as the methine proton alpha to two oxygens and one carbon atom in the lactol. The signal these researches attribute to SOZ may in fact be lactol- or hemiacetal-type structures.

### *4.2 Future Work*

***4.2.1 Aldehyde-Lactol Equilibrium Experiment*** Although no aldehyde has been detected, the formation of the lactol products may be in equilibrium with the preceding aldehyde structure in the mechanism. Reported equilibrium constants (*K*) for the closure of 4-hydroxybutanal and 5-hydroxypentanal to their cyclic hemiacetals have been reported as K = 8 and K = 16, respectively.[67] To determine if the lactol isomers found in the present study are in equilibrium with each other and with the open chain hydroxyl aldehyde, an NMR study of the effect of adding a crystal of p-toluene sulfonic acid to the product mixture should be conducted. If in fact they are in equilibrium, then the aldehyde is an intermediate and may react with other molecules in cloud droplets such as ammonium and amines.

***4.2.2 Closed System Aqueous Kinetics*** The present research was conducted in an open system, meaning that ozone was able to flow out of the system and water was able to evaporate during the reaction. A study with humidified air using a water bubbler should be conducted in order to determine more accurate kinetics information. It is hypothesized that closing the system will not change what products form, but perhaps it may impact product ratios.

***4.2.3 DRIFTS Experiment*** Although the present study included conducting the reaction on inorganic aerosols, a more robust model of the interaction of α-terpineol and inorganic aerosols should be studied. A proven method for this involves coating mineral

dusts and sea salts (NaCl) with α-terpineol, exposing it to ozone, and monitoring with infrared spectroscopy. Coating of kaolinite and α-alumina (mineral dusts) with limonene (organic aerosol) has been successfully monitored with Diffuse Reflectance Infrared Spectroscopy (DRIFTS).[68]

***4.2.4 O-18 experiment*** For additional verification of the product identification and mechanism, a study with isotopically-labeled ozone can be conducted. Labeling ozone with $^{18}O$ may provide information on where O atoms in the products originate—from ozone, α-terpineol's alcohol group, or water. The mechanism in Scheme 9 is hypothetically labeled with red markers to indicate the locations of $^{18}O$ in the structures.

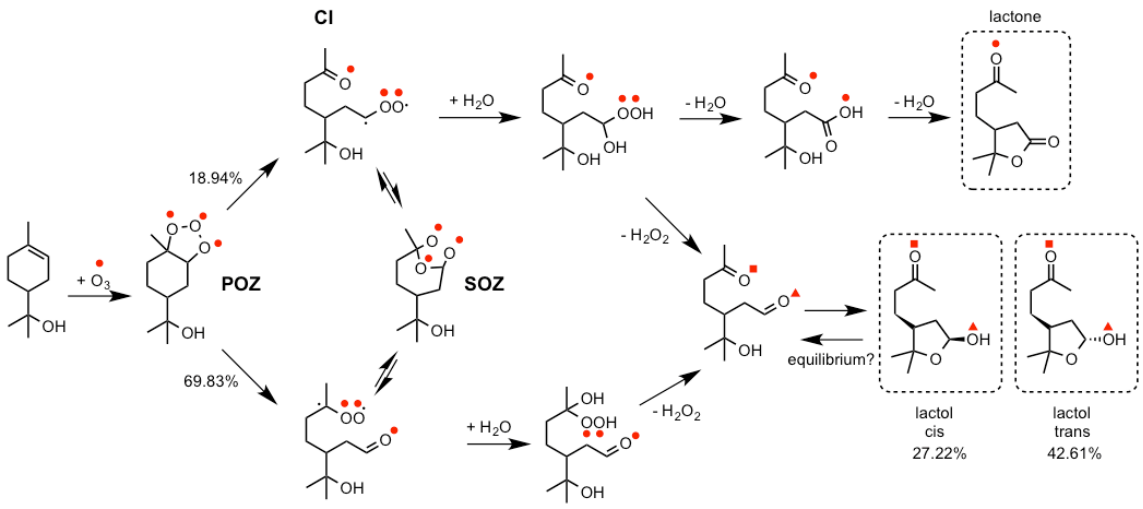


**Scheme 9.** Proposed mechanism with hypothetical locations of isotopically marked oxygen atoms. Red markers indicate location of $^{18}O$. In formation of lactol, red squares indicate where $^{18}O$ would be via the top pathway and the red triangles indicate where $^{18}O$ would be via the bottom pathway. Both labeled oxygen atoms would not be present at the same time.

Oxygen atoms not labeled with red markers indicate the locations of $^{16}O$. In the mechanism, after the pathways converge in the formation of lactol, the red squares indicate where $^{18}O$ would be via the top pathway and the red triangles indicate where $^{18}O$

would be via the bottom pathway. The labeled oxygen atoms would not be present in the same structure.

After conducting the experiment, the product mixture should be analyzed with Gas Chromatography/Mass Spectrometry (GCMS). The $^{18}O$ replacing $^{16}O$ will shift the weights of the fragments in the mass spectra up by two mass units for every $^{18}O$ atom. To utilize these results, they must be compared with the known fragmentation of the products discussed in Chapter 3. Another technique to differentiate between isotopically-labeled oxygen and not isotopically-labeled oxygen is Infrared Spectroscopy (IR). It would be expected to see a shift in the C=O band on the IR spectrum due to $^{18}O$ instead of $^{16}O$. However, multiple products contain C=O bonds and are in mixture, which makes it too complicated to use IR with this experiment.

Each oxygen atom in the labeled ozone will be $^{18}O$. After the 1,3-cycloadditon of ozone to α-terpineol, two possible Criegee intermediates form—a primary radical shown in the top pathway of the mechanism and a secondary radical in the bottom pathway of the mechanism. Through the top pathway, the lactone is formed and only the oxygen of the ketone is expected to be labeled with $^{18}O$. If the lactol isomers are formed through the top pathway, then they are only expected to have the same oxygen as the lactol labeled. However, if the lactol isomers are formed through the bottom pathway, then only the oxygen of the alcohol is expected to be labeled with $^{18}O$. Although the lactol has two labeling possibilities, it is not expected to have both oxygen atoms labeled on the same structure because the two labels result from two different pathways.

In any of the products, only one oxygen atom is expected to be labeled at a time. Therefore, this experiment has a built-in control in which the parent ion and fragments containing the labeled oxygen atoms are only expected to shift up by two mass units. If both potentially labeled oxygen atoms in lactol were labeled at the same time, the mass would shift by four units. This is not expected; however, if it were observed, it would suggest that the mechanism would need to be modified.

It is important to note that some fragments of the lactone and lactol are similar, such as m/z = 43 and 71 which contain the ketone. When labeled, these fragments are expected to appear as m/z = 45 and 73. The fragments m/z = 43 and 71 would still be expected to appear as the ketone on the lactol is not labeled via the bottom pathway. The fragments m/z = 128 and 185, which are uniquely identified as fragments of the lactol, are expected to shift up to m/z = 130 and 187, and these fragments would correlate to lactol formation via the bottom pathway.

### *4.3 Recommendations*

The results of this study suggest greater significance of aqueous phase reactions in the atmosphere than gas phase reactions in the atmosphere, which is consistent with recent literature. Because there is comparatively less knowledge on aqueous phase atmospheric reactions than there is on that of the gas phase, the results of the present study emphasize the importance of studying aqueous phase atmospheric reactions and aqueous phase ozonolysis in particular.

Limited policy recommendations can be made. Nothing can be done about plants emitting organic aerosols like α-terpineol. These emissions in and of themselves are

largely not detrimental to the planet. However, the reactions between the emitted organic aerosols and oxidizing agents such as ozone have climate, health, and visibility impacts. The abundant presence of oxidizing agents is the result of pollution by man, which can and should be regulated to reduce the occurrence and impact of their reactions with organic aerosols.

**References**

1. Beijing, U. S. E. i. U.S. Embassy Beijing Air Quality Monitor. http://beijing.usembassy-china.org.cn/aqirecent3.html.
2. World Health Organization. Regional Office for, E.; World Health, O., *Air quality guidelines: global update 2005: particulate matter, ozone, nitrogen dioxide, and sulfur dioxide*. World Health Organization: 2006.
3. Wang, Q.; Shao, M.; Zhang, Y.; Wei, Y.; Hu, M.; Guo, S., Source apportionment of fine organic aerosols in Beijing. *Atmospheric Chemistry and Physics* **2009,** *9* (21), 8573-8585; Yu, L.; Wang, G.; Zhang, R.; Zhang, L.; Song, Y.; Wu, B.; Li, X.; An, K.; Chu, J., Characterization and source apportionment of PM2. 5 in an urban environment in Beijing. *Aerosol and air quality research* **2013,** *13* (2), 574-583.
4. Hallquist, M.; Wenger, J. C.; Baltensperger, U.; Rudich, Y.; Simpson, D.; Claeys, M.; Dommen, J.; Donahue, N. M.; George, C.; Goldstein, A. H., The formation, properties and impact of secondary organic aerosol: current and emerging issues. *Atmospheric Chemistry and Physics* **2009,** *9* (14), 5155-5236.
5. Goldstein, A. H.; Galbally, I. E., Known and unexplored organic constituents in the earth's atmosphere. *Environmental Science & Technology* **2007,** *41* (5), 1514-1521.
6. Sindelarova, K.; Granier, C.; Bouarar, I.; Guenther, A.; Tilmes, S.; Stavrakou, T.; Müller, J. F.; Kuhn, U.; Stefani, P.; Knorr, W., Global data set of biogenic VOC emissions calculated by the MEGAN model over the last 30 years. *Atmospheric Chemistry and Physics* **2014,** *14* (17), 9317-9341.
7. Records, G. W., Animals. In *Guinness World Records 2016*, Glenday, C., Ed. Jim Pattison Group: 2015; pp 28-49.
8. Malm, W. C., Introduction to visibility (Air Resources Division, National Park Service, Cooperative Institute for Research in the Atmosphere [CIRA], NPS Visibility Program). *Fort Collins: Colorado State University* **1999**.
9. Myhre, G.; Shindell, D.; Bréon, F. M.; Collins, W.; Fuglestvedt, J.; Huang, J.; Koch, D.; Lamarque, J. F.; Lee, D.; Mendoza, B., Anthropogenic and natural radiative forcing. In *Climate Change 2013: The Physical Science Basis. Contribution of Working Group I to the Fifth Assessment*
*Report of the Intergovernmental Panel on Climate Change*, Stocker, T. F., D. Qin, G.-K. Plattner, M. Tignor, S.K. Allen,; J. Boschung, A. N., Y. Xia, V. Bex and P.M. Midgley, Eds. Cambridge University Press: New York, 2013; pp 659-740.
10. Pöschl, U., Atmospheric aerosols: composition, transformation, climate and health effects. *Angewandte Chemie International Edition* **2005,** *44* (46), 7520-7540.
11. Israelachvili, J. N.; Pashley, R. M., Molecular layering of water at surfaces and origin of repulsive hydration forces. **1983**.
12. Service, N. W. All About Clouds. http://www.srh.noaa.gov/srh/jetstream/clouds/cloudwise/learn.html.
13. Charlson, R. J.; Seinfeld, J. H.; Nenes, A.; Kulmala, M.; Laaksonen, A.; Facchini, M. C., Reshaping the theory of cloud formation. *Science* **2001,** *292* (5524), 2025-2026.
14. Graham, S. Clouds & Radiation *Earth Observatory* [Online], 1999. http://earthobservatory.nasa.gov/Features/Clouds/.

15. Usher, C. R.; Michel, A. E.; Grassian, V. H., Reactions on mineral dust. *Chemical reviews* **2003,** *103* (12), 4883-4940.
16. Boldo, E.; Medina, S.; Le Tertre, A.; Hurley, F.; Mücke, H.-G.; Ballester, F.; Aguilera, I., Apheis: Health impact assessment of long-term exposure to PM2. 5 in 23 European cities. *European journal of epidemiology* **2006,** *21* (6), 449-458.
17. Wang, T.; Kwok, J. Y. H., Measurement and analysis of a multiday photochemical smog episode in the Pearl River Delta of China. *Journal of Applied Meteorology* **2003,** *42* (3), 404-416.
18. Manahan, S. E., Photochemical Smog. In *Environmental Chemistry*, 8th ed.; CRC Press: New York, 2005.
19. Husar, R. B., Atmospheric Aerosol Science Before 1900. In *History of Aerosol Science*, Preining, O.; Davis, E. J., Eds. Austrian Academy of Sciences: Vienna, 2000.
20. Fuzzi, S.; Andreae, M. O.; Huebert, B. J.; Kulmala, M.; Bond, T. C.; Boy, M.; Doherty, S. J.; Guenther, A.; Kanakidou, M.; Kawamura, K., Critical assessment of the current state of scientific knowledge, terminology, and research needs concerning the role of organic aerosols in the atmosphere, climate, and global change. *Atmospheric Chemistry and Physics* **2006,** *6* (7), 2017-2038.
21. Ainsworth, E. A.; Yendrek, C. R.; Sitch, S.; Collins, W. J.; Emberson, L. D., The effects of tropospheric ozone on net primary productivity and implications for climate change*. *Annual review of plant biology* **2012,** *63*, 637-661.
22. Bailey, P. S., Introduction. In *Ozonation in Organic Chemistry*, Academic Press: New York, 1978; Vol. I, pp 1-5.
23. Pinder, A. R., Monocyclic Monoterpenes. In *The Chemistry of the Terpenes*, Wiley: New York, 1960; pp 42-82.
24. Johnson, D.; Marston, G., The gas-phase ozonolysis of unsaturated volatile organic compounds in the troposphere. *Chemical Society Reviews* **2008,** *37* (4), 699-716.
25. Miller, A.; Soloman, P. H., Pericyclic Reactions. In *Writing Reaction Mechanisms in Organic Chemistry*, 2nd ed.; Academic Press: New York, 2000; pp 343-416.
26. Ess, D. H.; Houk, K. N., Theory of 1,3-Dipolar Cycloadditions: Distortion/Interaction and Frontier Molecular Orbital Models. *Journal of the American Chemical Society* **2008,** *130* (31), 10187-10198.
27. Fukui, K., The role of frontier orbitals in chemical reactions. *Nobel Lectures Chemistry: 1981-1990* **1992**, 9-26.
28. Bailey, P. S., Ozonolysis of Olefins: Routes to Peroxidic Products. In *Ozonation in Organic Chemistry*, Academic Press: New York, 1978; Vol. I, pp 45-82.
29. Nangia, P. S.; Benson, S. W., Thermochemistry and kinetics of ozonation reactions. *Journal of the American Chemical Society* **1980,** *102* (9), 3105-3115.
30. Bailey, P. S., Ozonolysis of Olefins: The Peroxidic Products. In *Ozonation in Organic Chemistry*, Academic Press: New York, 1978; Vol. I, pp 25-43.
31. Vibenholt, A.; Nørgaard, A. W.; Clausen, P. A.; Wolkoff, P., Formation and stability of secondary ozonides from monoterpenes studied by mass spectrometry. *Chemosphere* **2009,** *76* (4), 572-577.

32. Carey, F. A.; Sundberg, R. J., Ozonolysis. In *Advanced Organic Chemistry: Part B: Reactions and Synthesis*, 4th ed.; Kluwer Academic/Plenum Publishers: New York, 2001; pp 788-790.
33. McMurry, J., Alkenes: Reaction and Synthesis. In *Organic Chemistry*, Cengage Learning: 2012; pp 262-313.
34. Enami, S.; Hoffmann, M. R.; Colussi, A. J., Prompt formation of organic acids in pulse ozonation of terpenes on aqueous surfaces. *The Journal of Physical Chemistry Letters* **2010,** *1* (15), 2374-2379.
35. Wang, H. L.; Huang, D.; Zhang, X.; Zhao, Y.; Chen, Z. M., Understanding the aqueous phase ozonolysis of isoprene: distinct product distribution and mechanism from the gas phase reaction. *Atmospheric Chemistry and Physics* **2012,** *12* (15), 7187-7198.
36. Forester, C. D.; Wells, J. R., Yields of carbonyl products from gas-phase reactions of fragrance compounds with OH radical and ozone. *Environmental science & technology* **2009,** *43* (10), 3561-3568.
37. Wells, J. R., Gas-phase chemistry of $\alpha$ -terpineol with ozone and OH radical: Rate constants and products. *Environmental science & technology* **2005,** *39* (18), 6937-6943.
38. Zhang, X.; Chen, Z.; Wang, H.; He, S.; Huang, D., An important pathway for ozonolysis of alpha-pinene and beta-pinene in aqueous phase and its atmospheric implications. *Atmospheric Environment* **2009,** *43* (29), 4465-4471.
39. Barnum, T. J.; Medeiros, N.; Hinrichs, R. Z., Condensed-phase versus gas-phase ozonolysis of catechol: A combined experimental and theoretical study. *Atmospheric Environment* **2012,** *55*, 98-106.
40. Pflieger, M.; Goriaux, M.; Temime-Roussel, B.; Gligorovski, S.; Monod, A.; Wortham, H., Validation of an experimental setup to study atmospheric heterogeneous ozonolysis of semi-volatile organic compounds. *Atmospheric Chemistry and Physics* **2009,** *9* (6), 2215-2225.
41. Al Rashidi, M. J.; Chakir, A.; Roth, E., Heterogeneous ozonolysis of folpet and dimethomorph: a kinetic and mechanistic study. *The Journal of Physical Chemistry A* **2013,** *117* (14), 2908-2915.
42. Chen, Z. M.; Jie, C. Y.; Li, S.; Wang, H. L.; Wang, C. X.; Xu, J. R.; Hua, W., Heterogeneous reactions of methacrolein and methyl vinyl ketone: Kinetics and mechanisms of uptake and ozonolysis on silicon dioxide. *Journal of Geophysical Research: Atmospheres (1984–2012)* **2008,** *113* (D22).
43. Shu, S.; Morrison, G. C., Surface Reaction Rate and Probability of Ozone and Alpha-Terpineol on Glass, Polyvinyl Chloride, and Latex Paint Surfaces. *Environ. Sci. Technol.* **2011,** *45* (10), 4285-4292.
44. Maksymiuk, C. S.; Gayahtri, C.; Gil, R. R.; Donahue, N. M., Secondary organic aerosol formation from multiphase oxidation of limonene by ozone: mechanistic constraints via two-dimensional heteronuclear NMR spectroscopy. *Physical Chemistry Chemical Physics* **2009,** *11* (36), 7810-7818.
45. Lambert, J. B.; Mazzola, E. P., *Nuclear Magnetic Resonance Spectroscopy: An Introduction to Principles, Applications, and Experimental Methods*. Pearson Education, Inc.: Upper Saddle River, NJ, 2004; p 1-341.

46. Frisch, M.; Trucks, G. W.; Schlegel, H. B.; Scuseria, G. E.; Robb, M. A.; Cheeseman, J. R.; Scalmani, G.; Barone, V.; Mennucci, B.; Petersson, G. A.; Nakatsuji, H.; Caricato, M.; Li, X.; Hratchian, H. P.; Izmaylov, A. F.; Bloino, J.; Zheng, G.; Sonnenberg, J. L.; M. Hada; Ehara, M.; Toyota, K.; Fukuda, R.; Hasegawa, J.; Ishida, M.; Nakajima, T.; Honda, Y.; Kitao, O.; Nakai, H.; Vreven, T.; J. A. Montgomery, J.; J. E. Peralta, F. O., M. Bearpark, J. J. Heyd, E. Brothers,; K. N. Kudin, V. N. S., R. Kobayashi, J. Normand,; K. Raghavachari, A. R., J. C. Burant, S. S. Iyengar, J. Tomasi,; M. Cossi, N. R., J. M. Millam, M. Klene, J. E. Knox, J. B. Cross,; V. Bakken, C. A., J. Jaramillo, R. Gomperts, R. E. Stratmann,; O. Yazyev, A. J. A., R. Cammi, C. Pomelli, J. W. Ochterski,; R. L. Martin, K. M., V. G. Zakrzewski, G. A. Voth,; P. Salvador, J. J. D., S. Dapprich, A. D. Daniels,; O. Farkas, J. B. F., J. V. Ortiz, J. Cioslowski,; Fox, a. D. J., Gaussian 09. Gaussian, Inc. Wallingford, CT: 2009.

47. Queiroz, L. H. K.; Lacerda, V.; dos Santos, R. B.; Greco, S. J.; Cunha Neto, Á.; de Castro, E. V. R., NMR property calculations and experimental study of the 1, 6 - epoxycarvone and $\alpha$ - epoxypinene: a comparison of models. *Magnetic Resonance in Chemistry* **2011,** *49* (3), 140-146.

48. Keeler, J., Lecture 7 - Chapter 8: Two-dimensional NMR (I) by Dr James Keeler: "Understanding NMR spectroscopy". ANZMAG: 2013.

49. BSTFA + TMCS Product Specification. Sigma-Aldrich Co.: 1997.

50. Shu, Y.; Kwok, E. S. C.; Tuazon, E. C.; Atkinson, R.; Arey, J., Products of the gas-phase reactions of linalool with OH radicals, NO3 radicals, and O3. *Environmental science & technology* **1997,** *31* (3), 896-904.

51. Bailey, P. S., *Ozonation in Organic Chemistry*. Academic Press: New York, 1978; Vol. I.

52. Fuchs, P. L.; Bunnell, C. A., *Carbon-13 NMR based organic spectral problems*. Wiley New York: 1979.

53. Saier, E. L.; Cousins, L. R.; Basila, M. R., Infrared Determination of Aldehydes. An Improved Group Type Analysis. *Analytical Chemistry* **1962,** *34* (7), 824-826.

54. Donahue, N. M.; Drozd, G. T.; Epstein, S. A.; Presto, A. A.; Kroll, J. H., Adventures in ozoneland: down the rabbit-hole. *Physical Chemistry Chemical Physics* **2011,** *13* (23), 10848-10857.

55. Friedel, R. A.; Shultz, J. L.; Sharkey Jr, A. G., Mass spectra of alcohols. *Analytical Chemistry* **1956,** *28* (6), 926-934.

56. Sauer, F.; Schäfer, C.; Neeb, P.; Horie, O.; Moortgat, G. K., Formation of hydrogen peroxide in the ozonolysis of isoprene and simple alkenes under humid conditions. *Atmospheric Environment* **1999,** *33* (2), 229-241.

57. Finlayson-Pitts, B. J.; Pitts Jr, J. N., *Chemistry of the Upper and Lower atmosphere: Theory, Experiments, and Applications*. Academic Press: San Diego, 2000.

58. Angelini, M. M.; Garrard, R. J.; Rosen, S. J.; Hinrichs, R. Z., Heterogeneous reactions of gaseous HNO3 and NO2 on the clay minerals kaolinite and pyrophyllite. *The Journal of Physical Chemistry A* **2007,** *111* (17), 3326-3335.

59. Schütze, M.; Herrmann, H., Determination of phase transfer parameters for the uptake of HNO3, N 2 O 5 and O 3 on single aqueous drops. *Physical Chemistry Chemical Physics* **2002,** *4* (1), 60-67.

60. Johnson, P. N.; Davis, R. A., Diffusivity of ozone in water. *Journal of Chemical & Engineering Data* **1996,** *41* (6), 1485-1487.
61. Hoigné, J.; Bader, H., Rate constants of reactions of ozone with organic and inorganic compounds in water—I: non-dissociating organic compounds. *Water Research* **1983,** *17* (2), 173-183.
62. Bailey, P. S., Ozonolysis of Olefins: Initial Ozone Attack and Adduct. In *Ozonation in Organic Chemistry*, Academic Press: New York, 1978; Vol. I, pp 15-24.
63. Chen, Z. M.; Wang, H. L.; Zhu, L. H.; Wang, C. X.; Jie, C. Y.; Hua, W., Aqueous-phase ozonolysis of methacrolein and methyl vinyl ketone: a potentially important source of atmospheric aqueous oxidants. *Atmospheric Chemistry and Physics* **2008,** *8* (8), 2255-2265.
64. Brockbank, S. A.; Giles, N. F.; Rowley, R. L.; Wilding, W. V., Predicting Temperature-Dependent Aqueous Henry's Law Constants Using Group Contribution Methods. *Journal of Chemical & Engineering Data* **2013,** *59* (4), 1052-1061.
65. Agency, U. S. E. P. Patient Exposure and the Air Quality Index. https://www3.epa.gov/apti/ozonehealth/aqi.html.
66. Britigan, N.; Alshawa, A.; Nizkorodov, S. A., Quantification of ozone levels in indoor environments generated by ionization and ozonolysis air purifiers. *Journal of the Air & Waste Management Association* **2006,** *56* (5), 601-610.
67. Norman, R. O. C.; Coxon, J. M., Chemical Thermodynamics. In *Principles of organic synthesis*, CRC Press: 1993; p 16.
68. Staniec, A. R. Acid-Catalyzed Heterogeneous Reaction of Limonene with Mineral Aerosols: A New Mechanism for The Organic Coating of Inorganic Aerosols. Drew University, Madison, NJ, 2015.